Syntheses, Structures, and Spectro-electrochemistry of {Cp*(PP)Ru}C≡CC≡C{Ru(PP)Cp*} (PP = dppm, dppe) and Their Mono- and Dications†

Michael I. Bruce,*,‡ Benjamin G. Ellis,‡ Paul J. Low,§ Brian W. Skelton,⊥ and Allan H. White⊥

Department of Chemistry, University of Adelaide, Adelaide, South Australia 5005, Department of Chemistry, University of Durham, South Road, Durham DH1 3LE, England, and Department of Chemistry, University of Western Australia, Crawley, Western Australia 6009

Received January 9, 2003

The complexes $\{Cp^*(PP)Ru\}_2(\mu\text{-}C{\equiv}CC{\equiv}C)$ (PP = dppm **5a**, dppe **5b**) have been synthesized from RuCl(PP)Cp* (**1a**/**b**) via the corresponding vinylidenes $[Ru(=C=CH_2)(PP)Cp^*]^+$ (**2a**/**b**), deprotonation ($KOBu^t$) to the ethynyls Ru(C≡CH)(PP)Cp* (**3a**/**b**), oxidative coupling ($[FeCp_2][PF_6]$) to the bis(vinylidenes) $[\{Ru(PP)Cp^*\}_2\{\mu\text{-}(=C=CHCH=C=)\}]^{2+}$ (**4a**/**b**), and deprotonation [dbu (**4a**), $KOBu^t$ (**4b**)]. Electrochemistry of **5a/b** revealed the expected sequence of four 1e redox steps, which occurred at significantly lower $E°$ values than found for the $Ru(PPh_3)_2Cp$ analogue. Single-crystal X-ray structure determinations are reported for **1a**/**b**, **2a**/**b**, **3a**/**b**, **4a**/**b**, and **5a**/**b**, together with the oxidized products $[\mathbf{5b}][PF_6]_n$ (n = 1, 2). In the monocation $[\mathbf{5b}][PF_6]$ the Ru−C(1) [1.931(2) Å] and C−C distances [1.248−1.338(3) Å] are intermediate between those found in **5b** and the dication $[\mathbf{5b}]^{2+}$. The short Ru−C [1.857(5) Å] and experimentally equal C−C distances [1.269−1.280(6) Å] in $[\mathbf{5b}][PF_6]_2$ confirm the anticipated dicarbene-cumulene structure for the Ru=C=C=C=C=Ru bridge.

Introduction

Poly-ynyl and -diyl complexes are useful in the assembly of multimetallic structures because of their propensity to coordinate metals either by σ-bonding or by π-bonding. This chemical behavior, together with current interest in the properties of molecules containing metal−ligand fragments linked by unsaturated chains (molecular wires),[1] has resulted in the generation of a wide variety of such complexes. A structurally simple subset of poly-yndiyl compounds contains C_4 chains linking electron-rich metal centers, $\{L_nM\}$-C≡CC≡C-$\{ML_n\}$, as found for ML_n = Mo/W$(CO)_2$Tp,[2] MnX$(dmpe)_2$ (X = I, C≡CH),[3] Re(NO)(PR_3)Cp* (R = aryl),[4] Re$(CO)_3(Bu^t_2$-bpy),[5] Fe$(CO)_2$Cp*,[6] Fe(PP)Cp* (PP = dppe, dippe),[7] Ru(PPh_3)(L)Cp [L = PPh_3 (**5c**), PMe_3 (**5d**)],[8] $Ru_2(amp)_4$,[9] Rh/IrHCl$(PPr^i_3)_2$,[10] and PtCl$(P\text{-}Bu_3)_2$.[11] Several theoretical calculations have indicated that the HOMOs of some of these complexes consist of M−C antibonding orbitals lying above the remainder of the orbital manifold, with ionization potentials low enough to result in facile redox processes.[3,8b,12] Various reports have described the preparation of oxidized derivatives containing n+ cations (n = 1, 2, 3, or 4), although crystallographic characterization of many of these has proved difficult.

The valence structures **A**−**E** (Chart 1) can be used to rationalize the structures of the M−C_4−M bridges in these materials. Each form conceals a variety of subtle structural variations which can be related to more detailed and sophisticated accounts of their electronic structures. Ultimately, the structures are determined by the degree of interaction between the metal center and the carbon-based orbitals and are therefore a

† Dedicated to our friend and colleague Professor Martin Bennett, in recognition of his fine contributions to organometallic chemistry.

* Corresponding author. Fax: + 61 8 8303 4358. E-mail: michael.bruce@adelaide.edu.au.

‡ University of Adelaide.

§ University of Durham.

⊥ University of Western Australia.

(1) Paul, F.; Lapinte, C. *Coord. Chem. Rev.* **1998**, *178*−*180*, 427.

(2) Woodworth, B. E.; White, P. S.; Templeton, J. L. *J. Am. Chem. Soc.* **1997**, *119*, 828.

(3) (a) Kheradmandan, S.; Heinze, K.; Schmalle, H.; Berke, H. *Angew. Chem.* **1999**, *111*, 2412; *Angew. Chem., Int. Ed.* **1999**, *38*, 2270. (b) Fernandez, F. J.; Blacque, O.; Alfonso, M.; Berke, H. *Chem. Commun.* **2001**, 1266.

(4) (a) Zhou, Y.; Seyler, J. W.; Weng, W.; Arif, A. M.; Gladysz, J. A. *J. Am. Chem. Soc.* **1993**, *115*, 8509. (b) Seyler, J. W.; Weng, W.; Zhou, Y.; Gladysz, J. A. *Organometallics* **1993**, *12*, 3802. (c) Brady, M.; Weng, W.; Zhou, Y.; Seyler, J. W.; Amoroso, A. J.; Arif, A. M.; Böhme, M.; Frenking, G.; Gladysz, J. A. *J. Am. Chem. Soc.* **1997**, *119*, 775. (d) Meyer, W. E.; Amoroso, A. J.; Horn, C. R.; Jaeger, M.; Gladysz, J. A. *Organometallics* **2001**, *20*, 1115.

(5) Yam, V. W.-W.; Lau, V. C.-Y.; Cheung, K.-K. *Organometallics* **1996**, *15*, 1740.

(6) Akita, M.; Chung, M.; Sakurai, A.; Moro-oka, Y. *Chem. Commun.* **2000**, 1285.

(7) (a) Le Narvor, N.; Lapinte, C. *J. Chem. Soc., Chem. Commun.* **1993**, 357. (b) Le Narvor, N.; Toupet, L.; Lapinte, C. *J. Am. Chem. Soc.* **1995**, *117*, 7129. (c) Le Narvor, N.; Lapinte, C. *C. R. Acad. Sci. Paris, Ser. IIc* **1998**, 745. (d) Guillemot, M.; Toupet, L.; Lapinte, C. *Organometallics* **1998**, *17*, 1928.

(8) (a) Bruce, M. I.; Denisovich, L. I.; Low, P. J.; Peregudova, S. M.; Ustynyuk, N. A. *Mendeleev Commun.* **1996**, 200. (b) Bruce, M. I.; Low, P. J.; Costuas, K.; Halet, J.-F.; Best, S. P.; Heath, G. A. *J. Am. Chem. Soc.* **2000**, *122*, 1949.

(9) Ren, T.; Zhou, .; Alvarez, J. C. *Chem. Commun.* **2000**, 1197.

(10) (a) Gil-Rubio, J.; Laubender, M.; Werner, H. *Organometallics* **2000**, *19*, 1365. (b) Gil-Rubio, J.; Laubender, M.; Werner, H. *Organometallics* **1998**, *17*, 1202. (c) Werner, H.; Lass, R. W.; Gevert, O.; Wolf, J. *Organometallics* **1997**, *16*, 4077.

(11) Sonogashira, K.; Ohga, K.; Takahashi, S.; Hagihara, N. *J. Organomet. Chem.* **1980**, *188*, 237.

(12) Belanzoni, P.; Re, N.; Sgamellotti, A.; Floriani, C. *J. Chem. Soc., Dalton Trans.* **1998**, 1825.

10.1021/om030015g CCC: $25.00
Publication on Web 06/27/2003

function of the particular metal−ligand combination used to end-cap the carbon chain.

Chart 1

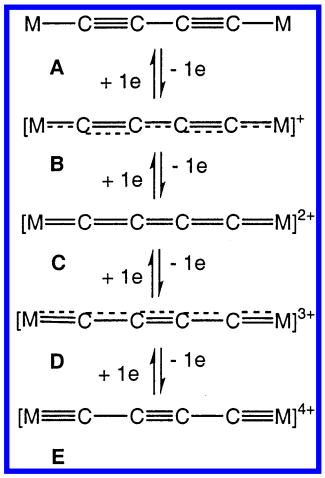

Others have examined the related chemistry of the rhenium and iron complexes mentioned above with the intriguing result that, while crystallographic and spectroscopic evidence favors a reduction in C≡C bond order and concomitant increase in C−C bond order as the rhenium complex is oxidized,[4c] Mössbauer spectroscopy and crystallographic studies of the iron complex suggest that it retains the diacetylenic nature of the C_4 ligand while generating Fe(III) centers.[7b] In particular, the trication in $[\{Fe(dippe)Cp^*\}_2(\mu\text{-}C_4)][OTf]_3$ features two Fe(III) centers and a carbon-centered (i.e., bridge-centered) radical.[7d] More recent crystallographic studies of the manganese system also gave results that are consistent with the generation of a cumulenic C_4 ligand in the $[\{MnI(dmpe)_2\}_2(\mu\text{-}C_4)]^{2+}$ dication,[3a] although in this case, the diyndiyl nature of the C_4 chain in the neutral complex is not so evident.

In previous papers we have described the redox chemistry of $\{Cp(PPh_3)(L)Ru\}_2(\mu\text{-}C{\equiv}CC{\equiv}C)$ [L = PPh_3, PMe_3] with the ultimate aim of characterizing a series of products related by one-electron steps which might exhibit the range of structures **A**−**E**.[8] While four 1e redox steps relating the 0/1+/2+/3+/4+ derivatives were found, only the neutral complex with R = Ph could be crystallographically characterized (as *cisoid* and *transoid* isomers).[13,14] In seeking to obtain similar derivatives that might be more readily accessible and therefore more convenient for physical measurements, we have increased the electron density at the ruthenium center by using strongly electron-donating ligands, such as pentamethylcyclopentadienyl (C_5Me_5, Cp*) and chelating diphosphines such as dppm and dppe. This paper reports a comparative study of complexes containing the Ru(PP)Cp* [PP = dppm (series **a**), dppe (series **b**)] groups, including X-ray structure determinations of the neutral and mono- and dications derived from the dppe complex. These confirm the predicted trend of a reduction in C≡C bond order and an increase in the C−C bond order represented by the valence structures **B** and **C**, respectively.

Results

Syntheses of $\{Cp^*(PP)Ru\}_2(\mu\text{-}C{\equiv}CC{\equiv}C)$ (PP = dppm, dppe). We have previously shown that the complex $\{Ru(PPh_3)_2Cp\}_2(\mu\text{-}C_4)$ is readily available via a fluoride-catalyzed desilylation of $Me_3SiC{\equiv}CC{\equiv}CSiMe_3$ in the presence of $RuCl(PPh_3)_2Cp$.[14] Although subsequently this reaction has been used to prepare several related complexes,[15] we have found that the analogous reaction does not proceed to any appreciable extent with RuCl(PP)Cp* (PP = dppm **1a**, dppe **1b**). Consequently, we have utilized the reaction sequence originally devised by Lapinte and co-workers to make the analogous iron diyndiyl complexes containing the Fe(dppe)Cp* group (Scheme 1).[7] These reactions, applied to RuCl(PP)Cp*, are described in the Experimental Section and do not require any detailed comment. All complexes have been fully characterized by elemental microanalyses, IR, NMR, and mass spectrometry and by single-crystal X-ray structural studies, as summarized below.

Accordingly, the chlorides **1a** and **1b**,[16] which are easily obtained from $RuCl(PPh_3)_2Cp^*$ and the diphosphine in refluxing toluene for 2 h, followed by column chromatography, were prepared with isolated yields of 83 and 95%, respectively. Conversion to the light yellow vinylidene complexes $[Ru(=C=CH_2)(PP)Cp^*][PF_6]$ (**2a/b**) was achieved by reactions of **1a/b** with $HC{\equiv}CSiMe_3$ in methanol in the presence of $[NH_4][PF_6]$ in 96 and 95% yields. If CH_2Cl_2 was used as the solvent for the reaction, reaction times were considerably longer [5 days (**2a**), 24 h (**2b**)] with lower yields of 62 and 74%, respectively. Deprotonation of **2a/b** with $KOBu^t$ afforded the bright yellow neutral ethynyl derivatives Ru(C≡CH)(PP)Cp* (**3a/b**) in essentially quantitative yield.

Oxidative coupling of the ethynyls to the bis(vinylidene) complexes $[\{Cp^*(PP)Ru\}_2(\mu\text{-}C{=}CHCH{=}C)][PF_6]_2$ (**4a/b**) occurred upon stirring **3a/b** with $[FeCp_2][PF_6]$ for 3 h at −78 °C. Slow addition of diethyl ether to the reaction mixture results in crystallization of the products as brick red crystalline solids in 91 and 85% yields, respectively. Deprotonation (dbu or $KOBu^t$) then afforded the desired butadiyndiyl compounds $\{Cp^*(PP)Ru\}_2(\mu\text{-}C{\equiv}CC{\equiv}C)$ (**5a/b**) as bright orange crystalline solids in 90% yield in each case. Although deprotonation of **4a** with dbu gave **5a** as the sole product, a mixture of products was obtained when $KOBu^t$ was used.

All complexes were readily identified from their spectroscopic properties. Most informative in the IR spectra were the bands found near 1625 [vinylidene ν(C=C)], 3265 and 1930 [ethynyl ν(≡CH) and ν(C≡C)], 1600−1635 [vinylidene ν(C=C)], and 1970 cm^{-1} [ν(C≡C)] for **2a/b**, **3a/b**, **4a/b**, and **5a/b**, respectively. Of interest are the changes in the ^{13}C resonances of the carbon chain atoms as these conversions are realized. In **2a/b**, resonances for the vinylidene carbons are found at δ 344.54 and 344.21 (triplets, C_α) and at δ 102.26 and 102.65 (singlets, C_β). In the ethynyl derivatives, both carbons resonate as triplets, with C_α showing the larger J(CP) at δ 120.26 (22.8 Hz) and 120.58 (22.9 Hz). For **3a**, C_β gives a poorly resolved triplet at δ 93.01, whereas in **3b** this resonance is at δ 92.99 with the

(13) Bruce, M. I.; Hinterding, P.; Tiekink, E. R. T.; Skelton, B. W.; White, A. H. *J. Organomet. Chem.* **1993**, *450*, 209.
(14) Bruce, M. I.; Hall, B. C.; Kelly, B. D.; Low, P. J.; Skelton, B. W.; White, A. H. *J. Chem. Soc., Dalton Trans.* **1999**, 3719.
(15) Bruce, M. I.; Kelly, B. D.; Skelton, B. W.; White, A. H. *J. Organomet. Chem.* **2000**, *604*, 150.
(16) Luo, L.; Zhu, N.; Zhu, N.-J.; Stevens, E. D.; Nolan, S. P.; Fagan, P. J. *Organometallics* **1994**, *13*, 669.

Scheme 1

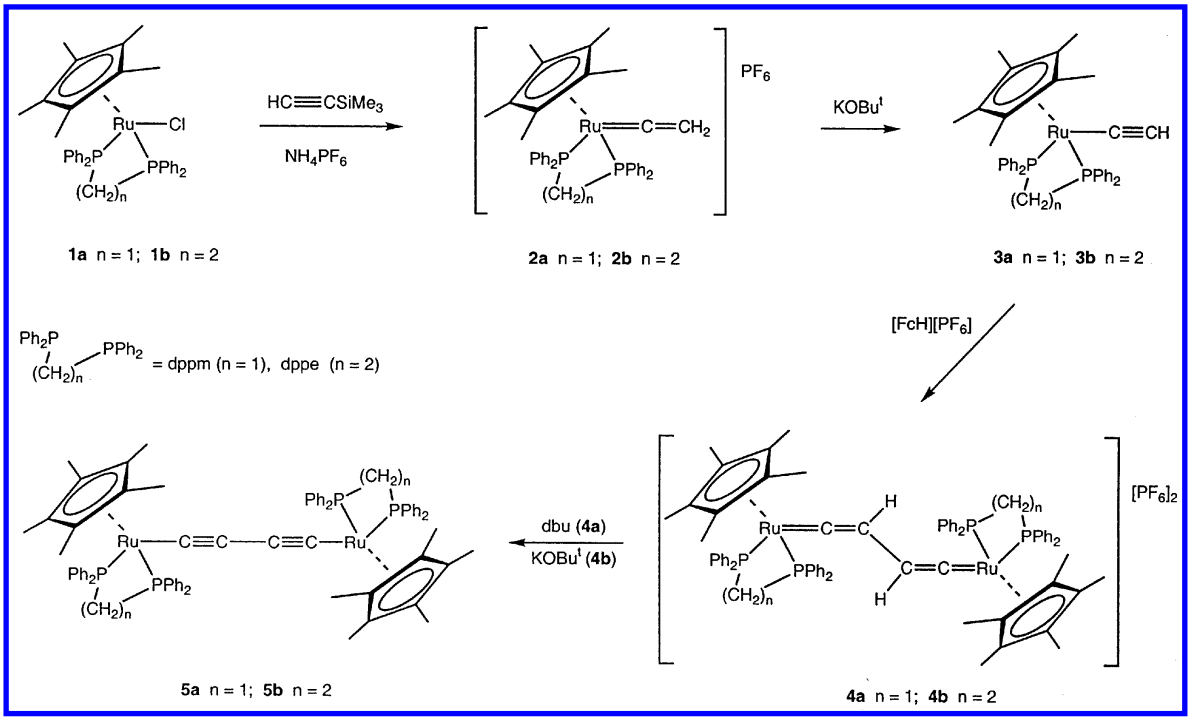

J(CP) coupling of 2.3 Hz being fully resolved. The bis(vinylidenes) **4a/b** also exhibit the characteristic downfield triplets at δ 348.59 and 348.08, with *J*(CP) of 15 and 17 Hz, respectively. In both cases, C_β resonated as a singlet at δ ca. 103. In the ^{31}P NMR spectra, resonances between δ 4.76 and 18.0 are found for the dppm complexes, while for the dppe derivatives, the signals occur between δ 75.92 and 82.53; if the PF_6^- anion is present, septet resonances at δ ca. −143 are present.

In the C_4 (diyndiyl) complexes strong IR ν(C≡C) absorptions are found at 1966 (**5a**) and 1973 (**5b**) cm^{-1}, while in the ^{1}H NMR spectrum, the Cp* methyl singlets are at δ 1.89 (**5a**) and 1.95 (**5b**). The CH_2 protons of the PP ligands resonate as multiplets at δ 4.23 (**5a**) or 1.95 and 2.71 (**5b**). In the ^{13}C NMR spectrum, the C_α triplets were found at δ 93.25 and 94.63 [*J*(CP) 27 Hz], while C_β was upfield at δ 100.38 and 99.47 (both singlets), respectively. There are again significant differences in the ^{31}P chemical shifts, with singlets at δ 17.50 (**5a**) or 82.53 (**5b**). The ES mass spectra contain M^+ ions at *m*/*z* 1290 and 1318, respectively, together with [Ru(PP)Cp*]$^+$.

Molecular Structures. Figures 1−3 contain plots of single molecules or cations of each of the complexes studied, while selected structural parameters are collected in Table 1. In **1a/b**, the major difference is found in the Ru−C(Cp*) distances, which average 2.20(2) and 2.24(1) Å, respectively, the result of the more compact diphosphine ligand in the former, also reflected in the smaller bite angle P(1)−Ru−P(2) of 71.53(6)° versus 82.15(2)° for the dppe analogue. The Ru−P distances are similar in both complexes [range 2.2812(5)−2.294(2) Å].

Similar differences in the P(1)−Ru−P(2) angles are found for the other complexes, with values for P(1)−Ru−P(2) ranging between 70.71(2)° and 71.74(2)° (dppm) and 81.50(3)° and 83.6(1)° (dppe). However, the average Ru−C(Cp*) distances all fall in the range 2.24(2)−2.29(3) Å with no apparent correlation with the diphosphine or the charge. In contrast, in the cationic derivatives **2a/b**, **4a/b**, [**5b**][PF_6], and [**5b**][PF_6]$_2$, the Ru−P distances [2.2756(5)−2.331(1) Å] are somewhat longer than those found in the neutral complexes **3a/b** and **5a/b** [2.2420(6)−2.2813(7) Å], probably because of reduced back-bonding from the cationic metal center to the phosphine ligand. The usual distorted octahedral structure is found for the ruthenium(II) center, with P−Ru−C angles ranging between 78.90(7)° and 87.50(6)°, seemingly independent of the nature of the ligands and charge.

The Ru−C(1) distances reflect the nature of the carbon ligand. For vinylidenes **2a/b**, short Ru−C distances [between 1.834(4) and 1.848(2) Å] correspond to a significant degree of multiple bonding between these atoms. In contrast, the σ-bonded alkynyl ligands in **3a/b** and **5a/b** are attached with longer Ru−C(1) distances, between 2.001(3) and 2.019(2) Å. Within the carbon ligands, C(1)−C(2) distances of 1.305(4) and 1.30(2) Å in **2a/b** and 1.338(7) and 1.323(5) Å in **4a**/**b** are consistent with the presence of formal C=C double bonds, while diminution to between 1.202(3) and 1.223(3) Å in **3a/b** and **5a/b** confirms the presence of C≡C triple bonds in these complexes. The central C−C bond lengths in **4a**/**b** [1.448(7), 1.470(5) Å] or **5a**/**b** [both 1.384(4) Å] are consistent with the conjugated structure of the C_4 ligands. The Ru−C(1)−C(2) angles are close to linear, ranging between 170.6(2)° and 177.1(3)°. The *E* configuration of the substituents on C(2)−C(3) in **4a**/**b** is also reflected in the torsion angles at these carbons of −174.2(6)° (**4a**) and −162.3(4)° (**4b**). Along the C_4 chains in **5a/b**, significant deviations from linearity occur, with angles at the carbon atoms of between 170.6(2)° and 179.1(2)°. The bending at each carbon is cumulative in each half of the molecule, with a total deviation from linearity of 3.2° (**5a**) or 5.1° (**5b**). This feature has been discussed elsewhere and results both

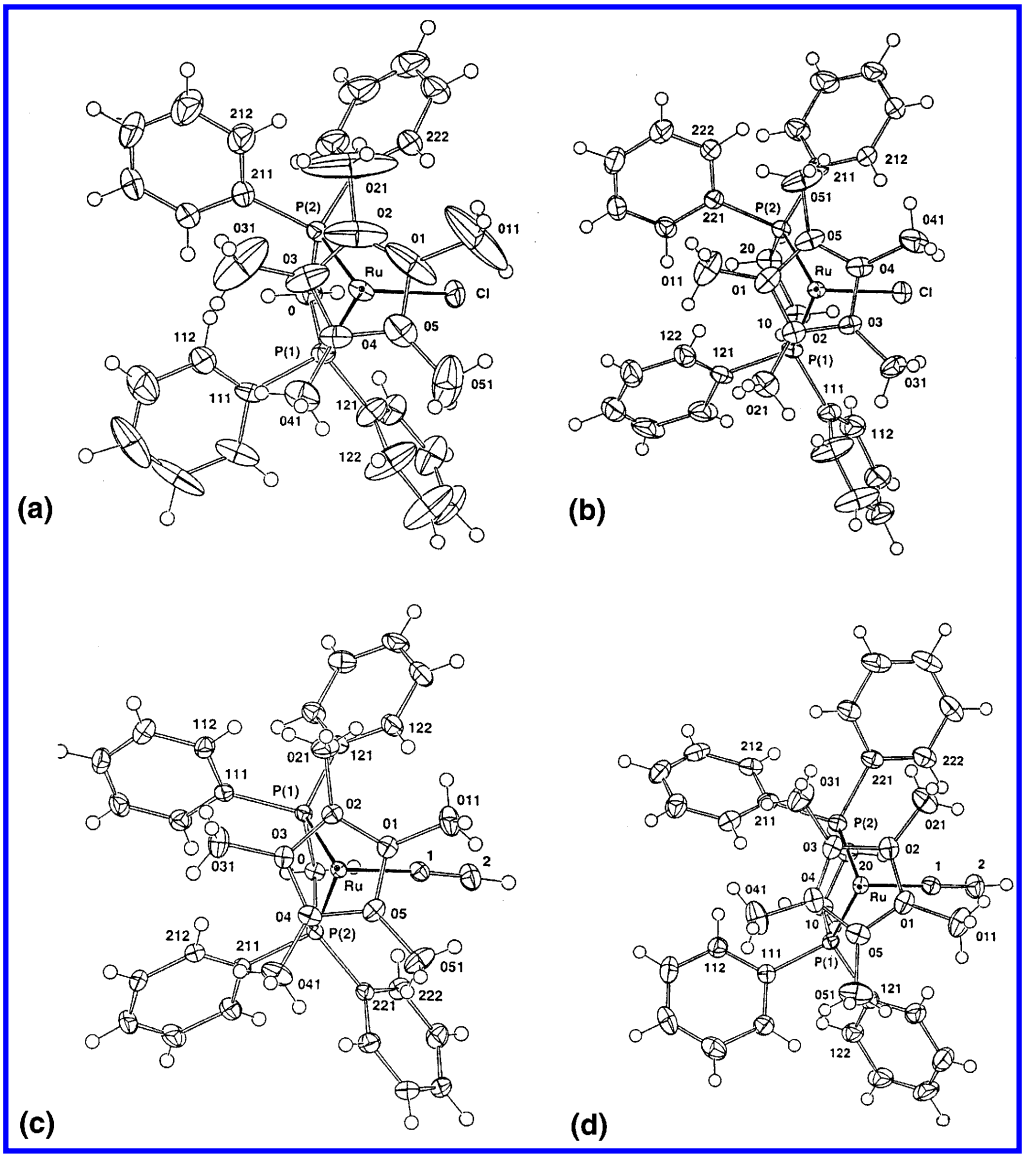

Figure 1. Projections of single molecules of (a) RuCl(dppm)Cp* (**1a**), (b) RuCl(dppe)Cp* (**1b**), (c) Ru(C≡CH)(dppm)Cp* (**3a**), and (d) Ru(C≡CH)(dppe)Cp* (**3b**).

from facile bending modes at C(sp) carbons and from contributions of different hybridized carbons in the metal-bonded systems.[17−19] In **5a/b**, the Ru−C_4−Ru chains approach a *transoid* configuration. The torsion angles between the Ru−Cp* axes are 69.9° and −46.9°.

Redox Chemistry. The redox potentials for complexes **1**−**4** are listed in Table 2. Single irreversible oxidation processes were found for **2a**/**b** at +1.71/+1.65 V and for **3a**/**b** at +0.225/+0.31 V (possibly corresponding to oxidative coupling to **4a**/**b**, although characteristic waves for the latter were not observed), while two reversible waves were found for both **4a**/**b** at +1.00, +1.26 V, respectively. The neutral complexes **1** and **3** with dppm are more readily oxidized than their dppe analogues, although the peak separations of the two differ. In the case of the chloro complexes, formation of a solvento cation by ionization of the Cl in solution cannot be ruled out, and this species may give rise to the irreversible wave found at higher potentials. Oxidation of **3** may result in irreversible formation of **4**, although no waves for **4** were found at higher potential. As expected, cationic complexes **2** and **4** are oxidized at higher potentials than the neutral species; in these cases, the dppe compounds are more easily oxidized. An irreversible process is found for **2**, whereas the lower of the two found for **4** is reversible. No reduction is found for any of the complexes within the solvent limit.

The rationale for this work is the search for Ru−C_4−Ru systems, which not only have lower oxidation potentials than previously described examples[8] but also afford more stable oxidized complexes which could be obtained in a crystalline form. Consequently, we have obtained cyclic voltammograms for **5a** and **5b** (Figure 4), and these results are summarized in Table 3, together with corresponding data for some related complexes. In the case of **5a** the first two oxidation processes are fully reversible [$i^a/i^c = 1$; current propor-

(17) Dembinski, R.; Lis, T.; Sazfert, S.; Mayne, C. L.; Bartik, T.; Gladysz, J. A. *J. Organomet. Chem.* **1999**, *578*, 229.
(18) (a) Peters, T. B.; Bohling, J. C.; Arif, A. M.; Gladysz, J. A. *Organometallics* **1999**, *18*, 3261. (b) Mohr, W.; Stahl, J.; Hampel, F.; Gladysz, J. A. *Inorg. Chem.* **2001**, *40*, 3263. (c) Bohling, J. C.; Peters, T. B.; Arif, A. M.; Hampel, F.; Gladysz, J. A. In *Coordination Chemistry at the Turn of the Century*; Ondrejovic, G., Sirota, A., Eds.; Slovak Technical Press: Bratislava, Slovakia, 1999; p 47.
(19) Bruce, M. I.; Costuas, K.; Halet, J.-F.; Hall, B. C.; Low, P. J.; Nicholson, B. K.; Skelton, B. W.; White, A. H. *J. Chem. Soc., Dalton Trans.* **2002**, 383.

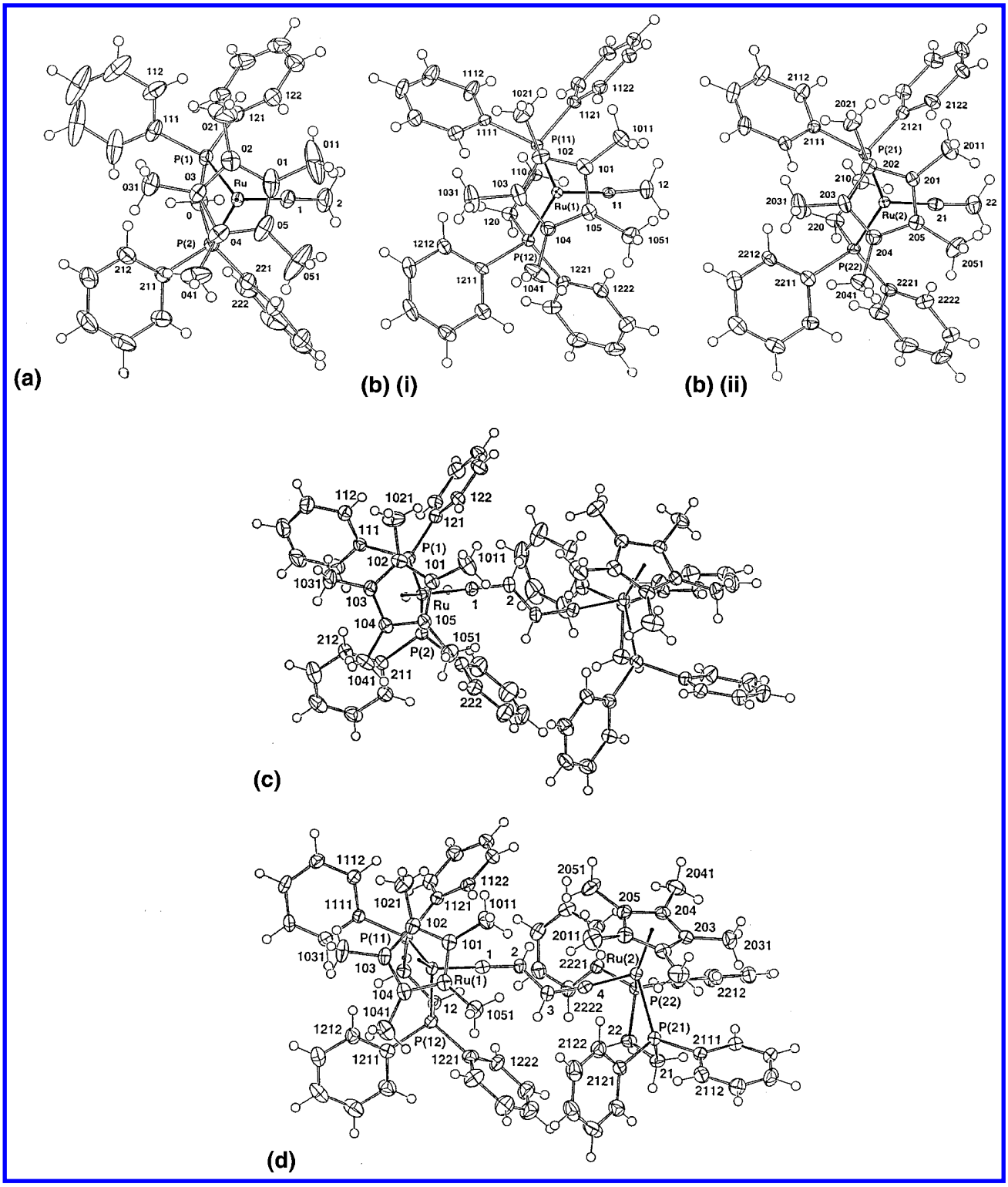

Figure 2. Projections of the cations of (a) [Ru(=C=CH$_2$)(dppm)Cp*][PF$_6$] (**2a**), (b) [Ru(=C=CH$_2$)(dppe)Cp*][PF$_6$] (**2b**) (two independent molecules), (c) [{Cp*(dppm)Ru}$_2$(=C=CHCH=C=)][PF$_6$]$_2$ (**4a**), and (d) [{Cp*(dppe)Ru}$_2$(=C=CHCH=C=)][PF$_6$]$_2$ (**4b**).

tional to (scan rate)$^{1/2}$]. The 2+/3+ oxidation wave in **5a** is only partially reversible ($i^a/i^c = 0.7$), while the 3+/4+ oxidation is chemically irreversible. In **5b**, the first three oxidations are reversible $i^a/i^c = 1$; current proportional to (scan rate)$^{1/2}$], with the 3+/4+ process being partially chemically reversible ($i^a/i^e = 0.7$).

As can be seen from Table 3, the first oxidation potentials for **5a** and **5b**, at −0.48 and −0.43 V, respectively, are lower than those determined for {Cp(PPh$_3$)(L)Ru}$_2$(μ-C$_4$) [L = PPh$_3$ (**5c**), PMe$_3$ (**5d**)], as expected. Comparison with the analogous iron complex shows that the 0/1+ potential of the latter, measured under the same conditions, occurs at an even lower value (−0.68 V). Similar comments apply to the second oxidation potentials (1+/2+) of these four complexes. However, as oxidation proceeds, the 2+/3+ couples are essentially identical for the four ruthenium compounds, while the 3+/4+ couples of **5a** and **5b** (at +1.41, +1.51

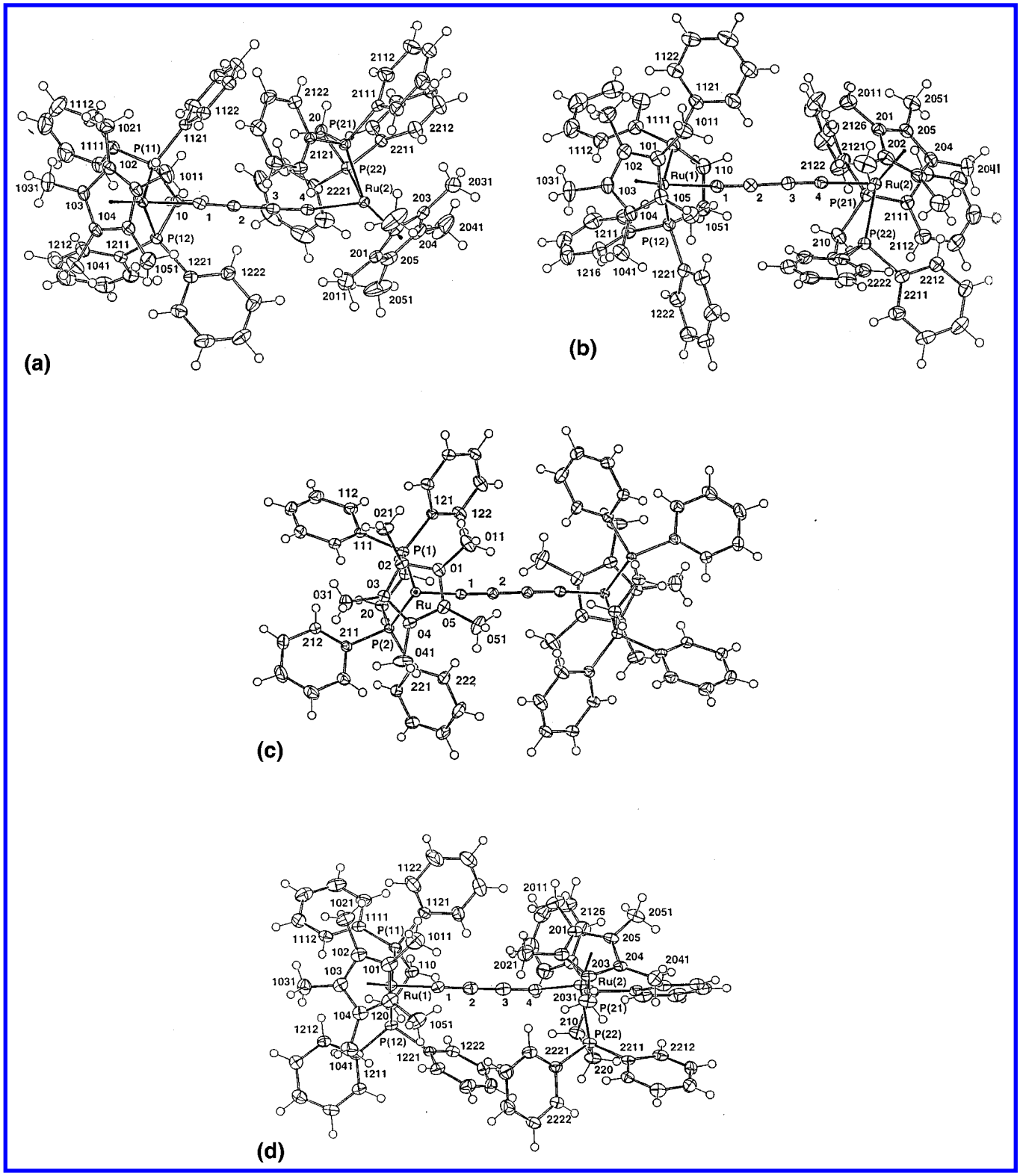

Figure 3. Projections of single molecules of (a) {Ru(dppm)Cp*}$_2$(μ-C$_4$) (**5a**) and (b) {Ru(dppe)Cp*}$_2$(μ-C$_4$) (**5b**) and the cations of (c) [{Ru(dppe)Cp*}$_2$(μ-C$_4$)][PF$_6$] ([**5b**]$^+$) and (d) [{Ru(dppe)Cp*}$_2$(μ-C$_4$)][PF$_6$]$_2$ ([**5b**]$^{2+}$).

V) bracket the value for **5d** [+1.46 V (irr.)]. The 3+/4+ couple has not been found in any related iron system to date.

In the case of the dppm complex **5a**, an unexpected peak (0.72 V) was observed in the cathodic sweep, which was found to decrease at higher scan rates. This is most likely due to a product resulting from the decomposition of the higher oxidized species under the conditions used in the experiment and is presently uncharacterized.

The high thermodynamic stability of the oxidized species [**5**]$^{n+}$ (n < 4) is evidenced by the significant separations of each redox process, giving rise to large comproportionation constants, K_C (**5a**: $n = 1$, $K_C = 4.46 \times 10^{10}$; $n = 2$, $K_C = 1.11 \times 10^{15}$; $n = 3$, $K_C = 1.80 \times 10^6$.

Table 1. Selected Structural Data

	1a dppm−Cl	**1b** dppe−Cl	**2a** dppm−CCH_2	**2b**[a] dppe−CCH_2	**3a** dppm−C≡CH	**3b** dppe−C≡CH
			Bond Distances (Å)			
Ru−P(1)	2.282(2)	2.2882(5)	2.2966(5)	2.320(3), 2.318(3)	2.2731(5)	2.2649(5)
Ru−P(2)	2.294(2)	2.2812(5)	2.2975(6)	2.317(3), 2.308(3)	2.2756(6)	2.2592(6)
Ru−C(Cp*)	2.185(9)−2.22(1)	2.219−2.252(2)	2.248−2.286(2)	2.27−2.30(1), 2.27−2.32(1)	2.219−2.263(2)	2.215−2.269(2)
(av)	2.20(2)	2.24(1)	2.27(2)	2.28(1), 2.28(2)	2.24(2)	2.25(2)
Ru−C(1)	2.434(2) [Cl]	2.4532(5) [Cl]	1.848(2)	1.85(1), 1.84(1)	2.015(2)	2.015(2)
C(1)−C(2)			1.305(4)	1.31, 1.29(2)	1.202(3)	1.202(3)
			Bond Angles (deg)			
P(1)−Ru−P(2)	71.53(6)	82.15(2)	71.74(2)	82.75(9), 83.6(1)	70.71(2)	82.71(2)
P(1)−Ru−C(1)	83.25(7) [Cl]	81.93(2) [Cl]	88.18(7)	83.5(3), 84.5(3)	87.97(6)	87.50(6)
P(2)−Ru−C(1)	87.59(7) [Cl]	90.93(2) [Cl]	85.54(7)	92.8(3), 92.3(4)	80.86(7)	85.27(6)
P(1)−C(0)−P(2)	92.7(3)		93.6(1)		90.78(9)	
Ru−C(1)−C(2)			176.2(2)	172.9(9), 172(1)	171.7(2)	173.7(2)

	4a $[dppm\text{-}C_4H_2]^{2+}$	**4b**[b] $[dppe\text{-}C_4H_2]^{2+}$
	Bond Distances (Å)	
Ru−P(1)	2.308(1)	2.331(1), 2.331(1)
Ru−P(2)	2.313(1)	2.310(1), 2.306(1)
Ru−C(Cp*)	2.262−2.312(5)	2.251−2.324(4), 2.268−2.311(4)
(av)	2.28(2)	2.29, 2.28(3)
Ru−C(1)	1.834(5)	1.837, 1.834(4)
C(1)−C(2)	1.338(7)	1.323, 1.324(5)
C(2)−C(3)	1.448(7)[c]	1.470(5)
	Bond Angles (deg)	
P(1)−Ru−P(2)	71.10(4)	82.38, 83.33(4)
P(1)−Ru−C(1)	88.1(2)	94.1, 91.0(1)
P(2)−Ru−C(1)	84.5(2)	80.9, 82.0(1)
P(1)−C(0)−P(2)	93.4(2)	
Ru−C(1)−C(2)	173.7(4)	170.9, 174.2(3)
C(1)−C(2)−C(3)	122.3(5)[c]	123.5, 123.6(4)

	5a[b] dppm-C_4	**5b**[b] dppe-C_4	**[5b]**$^+$ $[dppe\text{-}C_4]^+$	**[5b]**$^{2+}$ [b] $[dppe\text{-}C_4]^{2+}$
		Bond Distances (Å)		
Ru−P(1)	2.2633, 2.2697(6)	2.2556, 2.2420(8)	2.2756(5)	2.319, 2.312(1)
Ru−P(2)	2.2813, 2.2684(7)	2.2465, 2.2531(9)	2.3001(5)	2.311, 2.330(1)
Ru−C(Cp*)	2.226−2.259(2), 2.228−2.243(2)	2.219−2.278(3), 2.223−2.275(3)	2.232−2.291(2)	2.260−2.300(4), 2.262−2.309(3)
(av)	2.24(1), 2.234(6)	2.25, 2.25(2)	2.26(2)	2.27, 2.28(2)
Ru−C(1)	2.017, 2.019(2)	2.001, 2.003(3)	1.931(2)	1.858, 1.856(5)
C(1)−C(2)	1.216, 1.223(3)	1.223, 1.218(4)	1.248(3)	1.280, 1.269(7)
C(2)−C(3)	1.385(3)	1.382(4)	1.338(3)	1.294(7)
		Bond Angles (deg)		
P(1)−Ru−P(2)	70.72, 71.20(2)	81.50, 83.09(3)	81.89(2)	83.18, 81.93(4)
P(1)−Ru−C(1)	83.63, 80.14(7)	81.69, 82.54(8)	83.38(6)	85.0, 82.8(2)
P(2)−Ru−C(1)	78.90, 79.57(6)	84.25, 80.70(9)	93.45(6)	86.7, 92.5(1)
P(1)−C(0)−P(2)	91.02, 91.06(9)			
Ru−C(1)−C(2)	175.2, 170.6(2)	176.6, 177.1(3)	165.6(2)	175.6(5), 170.1(4)
C(1)−C(2)−C(3)	179.1(2), 177.7(3)	176.9, 178.0(3)	178.0(2)	176.7, 174.2(6)

[a] Values for molecules 1, 2 given. [b] Values involve Ru(1,2), C(1,4), C(2,3) as appropriate. [c] For C(3), read C(2′).

Table 2. Redox Potentials for 1−4[a]

complex	$E_{1/2}$
RuCl(dppm)Cp* **1a**	+0.245, +1.12[b]
RuCl(dppe)Cp* **1b**	+0.275, +1.34[b]
$[Ru(=C=CH_2)(dppm)Cp^*][PF_6]$ **2a**	+1.71[b]
$[Ru(=C=CH_2)(dppe)Cp^*][PF_6]$ **2b**	+1.65[b]
Ru(C≡CH)(dppm)Cp* **3a**	+0.225[b]
Ru(C≡CH)(dppe)Cp* **3b**	+0.31[b]
$[\{Ru(dppm)Cp^*\}_2(\mu\text{-}C{=}CHCH{=}C{=})_2][PF_6]_2$ **4a**	+1.00, +1.26
$[\{Ru(dppe)Cp^*\}_2(\mu\text{-}C{=}CHCH{=}C{=})_2][PF_6]_2$ **4b**	+1.00, +1.26

[a] CH_2Cl_2 solution, 0.1 M $[NBu_4]BF_4$. [b] Irreversible.

5b: $n = 1$, $K_C = 9.70 \times 10^{10}$; $n = 2$, $K_C = 7.26 \times 10^{13}$; $n = 3$, $K_C = 8.80 \times 10^7$). The CV data give estimates of thermodynamic stability and provide only an indication of chemical stability on the CV time scale; nevertheless we regarded the oxidized species $[\mathbf{5}]^{n+}$ ($n = 1-3$) to be viable synthetic targets.

Chemical oxidation of **5b** occurs with the marked color changes observed previously with **5c/d**. Treatment of the orange neutral compound with 1 or 2 equiv of $[FeCp_2][PF_6]$ affords the dark green monocation and intense dark blue dication. The former was obtained as the microcrystalline hexafluorophosphate, which is sensitive to air when in solution. As an odd-electron species, only broad resonances in the NMR spectra were observed, as expected, and these were assigned on the basis of their relative intensities: the C_5Me_5 resonance is at δ 10.72, while the methylene protons of the dppe ligand are found at δ 13.54. The phenyl protons appear

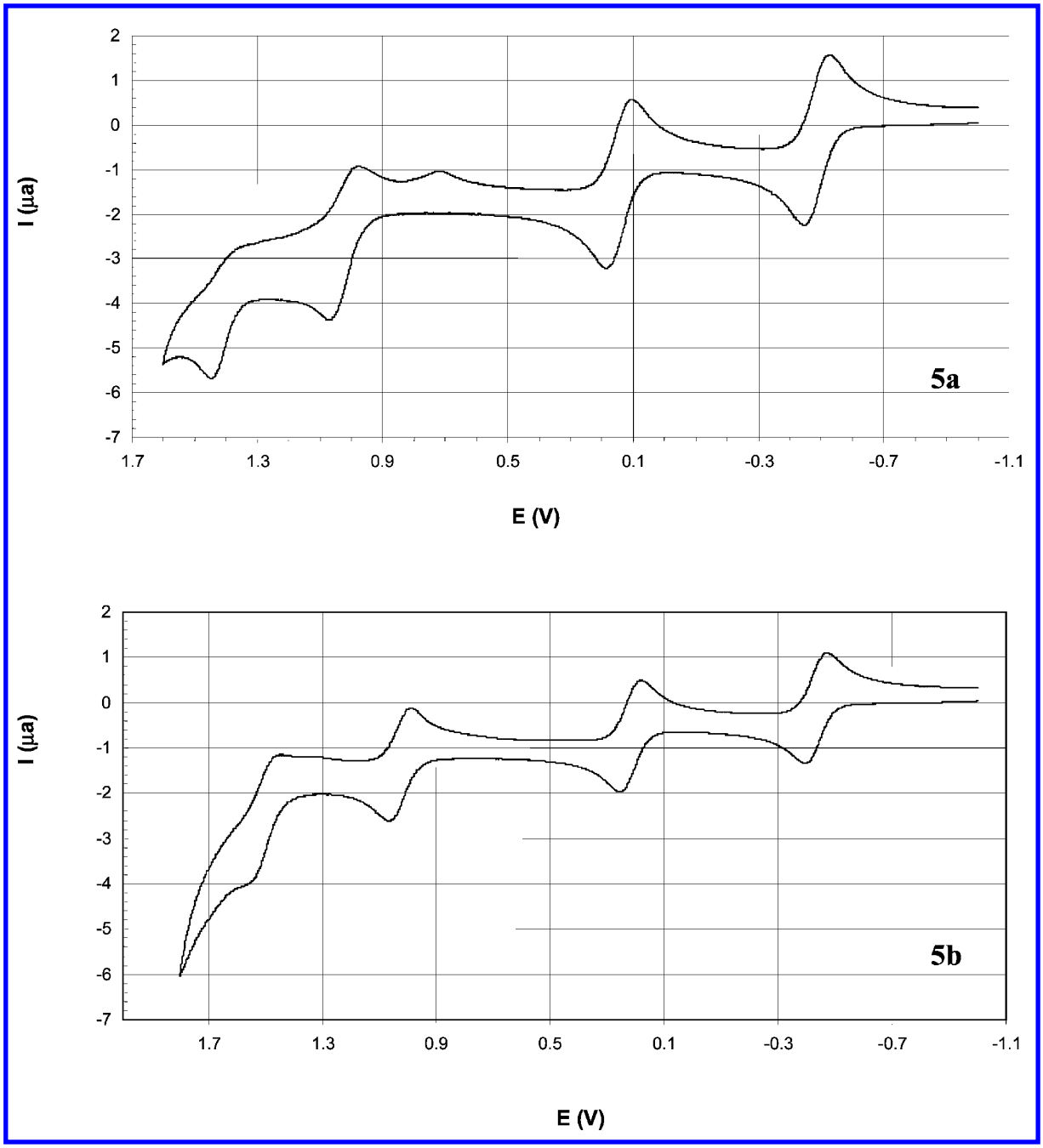

Figure 4. Cyclic voltammograms of {Ru(dppm)Cp*}$_2$(μ-C$_4$) (**5a**) and {Ru(dppe)Cp*}$_2$(μ-C$_4$) (**5b**), both taken at 200 mV s^{-1}.

as a set of broad multiplets between δ 6.46 and 7.92. No signal was observed in the ^{31}P NMR spectrum.

We have isolated and characterized the PF_6^- salt of [**5b**]$^{2+}$ as a dark blue solid, which exhibits a ν(CC) band at 1769 cm^{-1}, consistent with a further lowering of the CC bond order. In the ^{1}H NMR spectrum recorded in acetone-d_6, a sharp singlet for the Cp* protons is found at δ 1.94, while a broad singlet at δ 3.01 is assigned to the methylene protons of the dppe ligand. The phenyl protons appear in the expected region between δ 7.15 and 7.79. In the ^{13}C NMR spectrum, the Cp* carbons are singlets at δ 10.38 and 112.28, while multiplets at δ 27.79 and between δ 129.80 and 133.79 are assigned to the CH_2 and Ph carbons of the dppe ligand, respectively. Resonances for the C_4 moiety were not observed even with concentrated solutions and long delay times. In the ^{31}P NMR spectrum a slightly broadened singlet is seen at δ 117.89, while the PF_6 septet is observed at δ −143.20. The higher chemical shift of the P(dppe) nuclei, compared with **5b** (δ 82.53), is consistent with the removal of some electron density from the metal centers.

Figure 5 compares the ν(CC) bands of **5b**, recorded in CH_2Cl_2 as solvent, as oxidation proceeds. The neutral species gives a single band at 1963 cm^{-1} (with a shoulder at 1977 cm^{-1}), consistent with the presence of a C≡C triple bond. Upon oxidation to [**5b**]$^+$, a single ν(CC) band is present at 1860 cm^{-1}. In the spectrum of [**5b**]$^{2+}$ a single band at 1770 cm^{-1} is consistent with a further reduction in CC bond order; a very weak absorption at 1711 cm^{-1} is also present. In both oxidized species, a ν(PF) band at 838 cm^{-1} results from the PF_6

Table 3. Electrochemical Data for $[\{ML_n\}_2(\mu\text{-}C_4)]^{n+}$ (in CH_2Cl_2 unless otherwise stated; values referenced to $[FeCp_2]/[FeCp_2]^+ = 0.46$ V)

ML_n	E_1 (0/1+)	E_2 (1+/2+)	$\Delta E_{1/2}$°	E_3 (2+/3+)	E_4 (3+/4+)	K_C (0/1+/2+)	V_{AB}/eV	ref
Mn(C≡CH)(dmpe)$_2$ [a]	−1.46	−0.89	0.57			7.5×10^9		3b
MnI(dmpe)$_2$ [a]	−0.655	−0.020	0.64			5.4×10^{10}		3a
Re(NO)(PPh$_3$)Cp*	+0.01	+0.54	0.53			1.1×10^9		4d
Re(NO){P(tol)$_3$}Cp*	−0.22	+0.31	0.53			1.1×10^9	*d*	4d
Fe(dippe)Cp*	−0.97	−0.18	0.79	+0.81		2.25×10^{13}		7d
Fe(dppe)Cp*	−0.675	+0.045	0.72	+0.95		1.60×10^{12}	0.47	7a, 7b, 7d
Ru(dppm)Cp* **5a**	−0.48	+0.15	0.63	+1.04	+1.41[b]	4.46×10^{10}	0.63	this work
Ru(dppe)Cp* **5b**	−0.43	+0.22	0.65	+1.04	+1.51[c]	9.70×10^{10}	0.63	this work
Ru(PPh$_3$)$_2$Cp **5c**	−0.23	+0.41	0.64	+1.03	+1.68[c]	1.5×10^{11}	0.71	8b
Ru(PMe$_3$)(PPh$_3$)Cp **5d**	−0.26	+0.33	0.59	+0.97	+1.46[c]	2.1×10^{10}	0.69	8b

[a] MeCN. [b] Partially reversible. [c] Irreversible. [d] Values of 0.69, 0.61, 0.51 eV obtained from three absorption bands in NIR region (λ_{max} 891, 1020, 1225 nm, respectively).

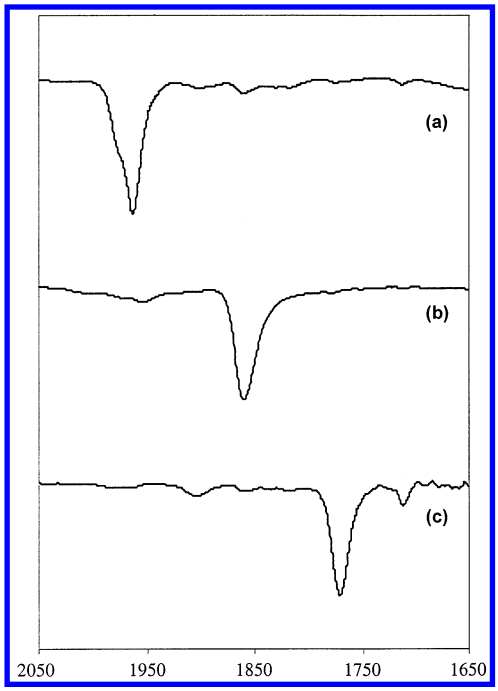

Figure 5. IR ν(CC) absorptions (in CH_2Cl_2) for (a) **5b**, (b) **[5b]**[PF_6], and (c) **[5b]**[PF_6]$_2$.

anion. The significant lowering of the ν(CC) absorption in these cations parallels the changes previously reported for the IR ν(CC) spectra of $\{Ru(PPh_3)_2Cp\}_2(\mu\text{-}C_4)$ (**5c**) and the mixed-ligand complex $\{Ru(PMe_3)(PPh_3)Cp\}_2(\mu\text{-}C_4)$ (**5d**) as oxidation proceeds. These changes are consistent with a decrease in C(1)−C(2) bond order. In turn, these results are anticipated from computational studies at the DF level, which suggest that electrons are removed from the HOMO, which is essentially Ru−C antibonding and delocalized over the Ru−C_4−Ru unit.[8b]

Crystals of the oxidized complexes **[5b]**[PF_6] (from CH_2Cl_2/hexane) and **[5b]**[PF_6]$_2$ (from ethanol) suitable for X-ray studies were obtained (see Figure 3, Table 1). The geometries of the cations are similar to those of the neutral complex, but detailed examination of the Ru−C_4−Ru bridges shows significant differences. In **[5b]**[PF_6] the structure of the centrosymmetric six-atom Ru−C_4−Ru chain is intermediate between the 1,3-diyndiyl structure found in neutral **5b** and the cumulenic structure in **[5b]**[PF_6]$_2$. In particular, the bond distances found in **[5b]**[PF_6] for Ru−C(1) [1.931(2) Å], C(1)−C(2) [1.248(3) Å], and C(2)−C(3) [1.338(3) Å] are equal to the averages of the corresponding values found in **5b** and **[5b]**[PF_6]$_2$. In the case of **[5b]**[PF_6]$_2$, the Ru−C(1) distances have decreased markedly to 1.858(4), 1.856(5) Å, while the C(1)−C(2) distances have increased to 1.280, 1.269(6) Å and the C(2)−C(2′) separation has decreased to 1.294(7) Å. These data are consistent with a change in electron distribution from the diyndiyl formulation **A** in **5b** to the cumulenic form **C** in **[5b]**[PF_6]$_2$. Comparison with previous structural studies of $[\{ML_n\}_2(\mu\text{-}C_4)]^{2+}$ cations (Table 4) shows that **[5b]**[PF_6]$_2$ provides the closest example so far to the pure cumulenic form anticipated for these group 8 systems, the C−C distances of **[5b]**[PF_6]$_2$ in particular being identical within 3σ. The dimensions are similar to those found in the manganese analogue $[\{MnI(dmpe)_2\}_2(\mu\text{-}C_4)]^{2+}$, in which the C−C separations along the bridge are 1.289, 1.295, and 1.298(5) Å, respectively.[3a] We note,

Table 4. Some Bond Parameters for $[\{ML_n\}_2(\mu\text{-}C_4)]^{x+}$ Complexes

$$\left[L_nM\text{—}C^1\text{—}C^2\text{—}C^3\text{—}C^4\text{—}ML_n\right]^{x+}$$

ML_n	x	M−C(1), M−C(4)	C(1)−C(2), C(3)−C(4)	C(2)−C(3)	M−C(1)−C(2), M−C(4)−C(3)	C(1)−C(2)-C(3), C(2)−C(3)-C(4)	ref
MnI(dmpe)$_2$	0	1.798(15)	1.263(17)	1.33(3)	176(1)	177(1)	3a
	1	1.763(2)	1.275(3)	1.313(5)	179(1)	179(1)	3a
	2	1.768(4), 1.770(4)	1.289, 1.298(5)	1.295(5)	171.9(5), 174.5(4)	173.9(4), 175.9(5)	3a
Re(NO)(PPh$_3$)Cp*	0	2.037(5)	1.202(7)	1.389(5)	174.4(5)	176.8(6)	4a, 4c
	2	1.909(7), 1.916(7)	1.263, 1.260(10)	1.305(10)	168.5, 171.4(7)	177.8, 175.4(9)	4a, 4c
Fe(dppe)Cp*	0	1.889(9), 1.885(8)	1.22, 1.22(1)	1.37(1)	175, 179(1)	177, 176(1)	a
	1	1.830(8)	1.236(9)	1.36(1)	167.0(6)	177(1)	7a, 7b
Ru(dppe)Cp* (**5b**)	0	2.001, 2.003(3)	1.223, 1.218(4)	1.382(4)	176.6, 177.1(3)	176.9, 178.0(3)	this work
	1	1.931(2)	1.248(3)	1.338(3)	165.6(2)	178.0(2)	this work
	2	1.858, 1.856(5)	1.280, 1.269(7)	1.294(7)	175.6, 170.1(4)	176.7, 174.2(6)	this work

[a] Lapinte, C. Private communication (2002).

Table 5. Near-Infrared and UV−Vis Spectral Data for [5a/b]$^{n+}$ (n = 1, 2)

	ν_{max} (cm^{-1})	ϵ (M^{-1} cm^{-1})	ΔV (cm^{-1})	ΔV calcd[a]	V_{AB} (eV)[b]
[**5a**]$^{+}$	10 165	14 000	2036	4846	0.63
	12 100	9500	2456	5287	
	14 215	3500	3720	5730	
[**5b**]$^{+}$	10 195	9850	2440	4853	0.63
	12 240	6600	2600	5317	
	14 000	2200	3800	5687	
[**5a**]$^{2+}$	15 385	17 600			
	17 452	5800			
	21 598	4350			
[**5b**]$^{2+}$	15 152	24 500			
	17 241	8000			
	21 505	4600			

[a] Calculated from eq 2. [b] Calculated from eq 1.

however, that in the neutral manganese complex, the C≡C bonds are already long [at 1.263(17) Å] and the central C−C bond short [at 1.33(3) Å].

Despite the changes in C−C bond lengths found in the ruthenium complexes, the angles at individual carbon atoms are closely similar in all cases and lie in the range 170.1−176.7(4)°, the complexes having transoid configurations. In [**5b**]$^{+}$ the torsion angle between the two vectors joining the Ru atoms with their Cp* rings is 180°, whereas in [**5b**]$^{2+}$, this angle is −39.7°. Note that an undistorted cumulenic C_4 chain would be expected to have a torsion angle of either 0° or 180°, so that the observed twisting is probably the result of packing effects. Other changes to the coordination about the ruthenium are minor, for example, the lengthening of the Ru−P distances [to 2.311, 2.319(1) Å] being comparable with those found in the other cations reported above. Progressive oxidation results in a steady decrease in the Ru···Ru separations from 7.821(1) (**5b**) to 7.6293(8) ([**5b**]$^{+}$) and 7.4757(1) Å ([**5b**]$^{2+}$).

UV/Vis/NIR Spectroscopy. To follow the oxidation processes, we undertook a UV/vis/NIR spectro-electrochemical study of the redox series [**5**]$^{n+}$. Samples were generated electrolytically in an OTTLE cell of design similar to that employed in our previous work.[8b] Not surprisingly, the electronic spectra of [**5a**]$^{n+}$ and [**5b**]$^{n+}$ are similar, not only to each other but also to those of [**5c**]$^{n+}$ and [**5d**]$^{n+}$. The discussion that follows refers to the compounds derived from **5a**, but the spectra and interpretation for **5b** are essentially the same (Table 5, Figure 6). Upon oxidation of **5a** to [**5a**]$^{+}$, a set of rather intense, overlapping broad bands are seen to grow in the NIR region, with discernible maxima at 810 and 965 nm. The observation of multiple bands in the NIR region has been reported previously for this class of complex.[4c,20] These bands were deconvoluted by fitting Gaussian plots, which allowed extraction of the parameters listed in Table 5. Higher energy shoulders observed for both **5c** and **5d** indicate that multiple bands are also present in the NIR spectra of these 35-electron half-sandwich ruthenium diyndiyl complexes.

Further oxidation results in the collapse of this set of NIR bands, with concomitant growth of new higher energy features at ca. 650, 573, and 463 nm, accompanied by an isosbestic point near 700 nm. This profile was found earlier for [**5c**]$^{2+}$ and [**5d**]$^{2+}$ and clearly points to all of the dications [**5**]$^{2+}$ having very

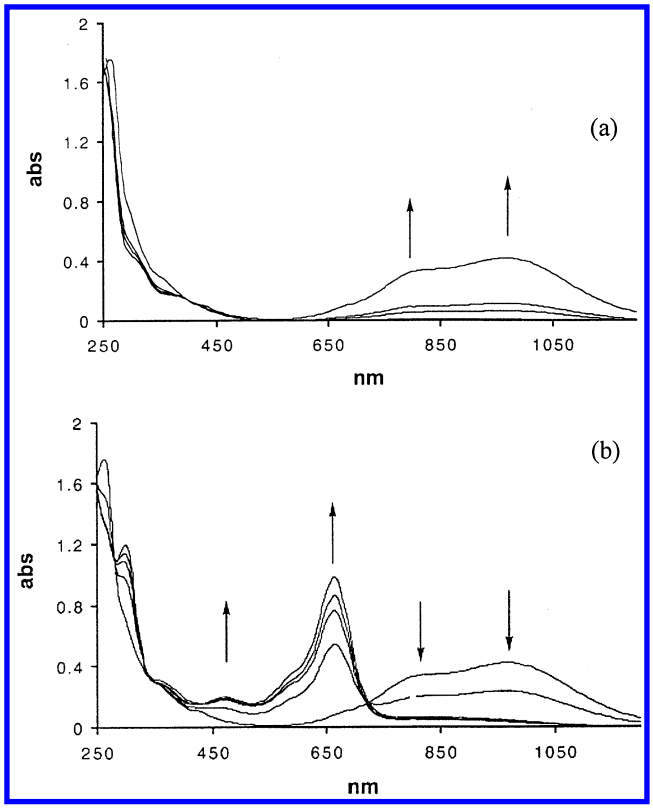

Figure 6. UV/vis/near-IR spectra of {Ru(dppm)Cp*}$_2$(μ-C_4) (**5a**) as oxidation proceeds: (a) **5a** to [**5a**]$^{+}$; (b) [**5a**]$^{+}$ to [**5a**]$^{2+}$.

similar underlying structures. Electrolytic reduction of these 34e dications proceeded smoothly and with complete chemical reversibility through the corresponding 35e monocations to the parent 36-electron species. However, while cyclic voltammetry indicated the high thermodynamic stability of the trications [**5a**]$^{3+}$ and [**5b**]$^{3+}$ with respect to disproportionation, these species proved to have significantly greater chemical reactivity than [**5c**]$^{3+}$ and [**5d**]$^{3+}$. Attempts to collect spectra from electrogenerated [**5a**]$^{3+}$ and [**5b**]$^{3+}$ within the OTTLE cell were unsuccessful as a result of rapid decomposition of the electrogenerated material, even at −30 °C.

Discussion

Application of the sequence of reactions outlined in Scheme 1 to the Ru(PP)Cp* series has allowed the synthesis and isolation of two new C_4 complexes, {Ru(PP)Cp*}$_2$$C_4$ (**5a/b**). X-ray structural characterization of all these complexes has been achieved. There are no exceptional features in the various precursors; further comments about the various forms of the C_4 complexes **5** are made below.

Of most interest is the redox behavior of these systems, which has been studied in detail using **5b**. CV data confirm the occurrence of four redox processes that relate the five species [{Ru(dppe)Cp*}$_2$$C_4$]$^{n+}$ (n = 0−4) through a series of 1e steps. IR studies of the ν(CC) frequencies have confirmed a decrease in C(1)−C(2) bond order as n increases from 0 to 2, the latter being consistent with a cumulenic arrangement. The NMR spectra confirm that the n = 0 species is diamagnetic and n = 2 predominantly so, whereas the monocation is paramagnetic. The somewhat broadened ^{31}P NMR

(20) Meyer, W. E.; Amoroso, A. J.; Horn, C. R.; Jaeger, M.; Gladysz, J. A. *Organometallics* **2001**, *20*, 1115.

signal for the dppe ligand in $[\mathbf{5b}]^{2+}$ possibly indicates that a small amount of the triplet state is in equilibrium with the singlet form. The predominantly singlet state of $[\mathbf{5b}][PF_6]_2$ is in marked contrast with the iron analogue.[7c] Of note in the present case is the significant reduction in $E(3+/4+)$, compared with **5c**/**d**. Although the CV data indicate only thermodynamic stabilities, we have been encouraged by these results to extend the preparative studies to these more highly charged species, which will be described elsewhere.

Symmetric odd-electron binuclear complexes are usually described as "mixed-valence" compounds, which in the case of the radical cations $[\mathbf{5}]^{+}$ and $[\mathbf{5}]^{3+}$ would formally contain Ru(II/III) (or d^6/d^5) and Ru(III/IV) (or d^5/d^4) centers, respectively. Similar mixed-valence complexes have been obtained by oxidation of the diyndiyl complexes containing Mn, Re, Fe, and Ru metal centers.[3,4,7,8] Mixed-valence compounds featuring multiple redox centers linked by some bridging ligand have been classified by Robin and Day[21] as belonging to one of three classes, distinguished by the degree of interaction between the redox centers. In class I materials, the redox centers are essentially independent and behave as such. Class II complexes display an intermediate degree of coupling between the redox centers and give rise not only to properties derived from the superposition of the valence-localized states but also to some unique spectroscopic features arising from electron transfer between the redox centers. The redox centers in class III materials are so strongly coupled that the system is better described in MO terms with a delocalized ground state. The spectroscopic properties of class III materials are unique and do not include the characteristics of the valence-localized limiting forms. Class II materials have been the subject of detailed theoretical treatments,[22] and recently the behavior of compounds that fall at the class II/III boundary have attracted a considerable degree of interest.[23−27]

Classical analyses of symmetric mixed-valence materials consider the construction of a potential energy surface from two parabolic functions representing the noninteracting centers. Electronic coupling between the centers results in an avoided crossing at the intersection of these parabolic functions. While a detailed description of the two adiabatic surfaces that result is beyond the scope of the present article (for an excellent discussion see ref 22), it is important to recognize that photoexcitation from the lower surface to the upper will result in an electronic absorption band, which corresponds to a transition from the (HOMO − 1) to the SOMO. Consequently, mixed-valence complexes often give rise to a low-energy electronic transition that is found in the NIR region. In the case of class II materials, this band is usually termed the intervalence charge transfer (IVCT) band and corresponds to the optically excited electron transfer between the two interacting redox centers.[22,25] More recently, the shapes of these potential energy surfaces have been the source of a large amount of detailed discussion.[24,25] The heavily overlapping NIR transitions in the present examples prevent our observing the low-energy side of the NIR bands and preclude a detailed analysis of the band shape. However, the classical analysis of the IVCT band maximum and shape in class II materials derived by Hush and others permits calculation of the electronic coupling parameter V_{AB} (or H_{AB}) from the band maximum (or energy) and the shape of the band on the high-energy side.[22−27]

For class III materials, in which the odd electron is delocalized over the redox centers, the coupling parameter V_{AB} is simply related to the energy of the NIR band.

$$V_{AB} = \nu_{max}/2 \qquad (1)$$

We are not the first to consider the term "inter-valence charge transfer" applied to class II mixed-valence complexes to be unduly cumbersome and potentially misleading when applied to delocalized class III complexes.[4c,25] However, in the absence of a more precise term, and in keeping with the current trends in the literature, we shall refer to the NIR absorption band in these systems using established IVCT terminology.

A simple test that is applied to distinguish class II and class III materials entails a comparison of the observed bandwidth $\nu_{1/2}$ of the lowest energy electronic transition with the value determined from the relationship

$$\nu_{1/2} = (2310\nu_{max})^{1/2} \qquad (2)$$

derived by Hush for class II complexes.[26] Class II materials usually give rise to IVCT bands that are either in good agreement with or broader than the Hush analysis predictions, while class III materials give rise to relatively sharp transitions. However, in the case of $[\mathbf{5a/b}]^{+}$ the presence of multiple, overlapping NIR absorptions, which can be deconvoluted to three closely spaced Gaussian absorptions, complicates this analysis. Nevertheless, the observation of electronic, vibrational, and NMR spectral profiles for $[\mathbf{5}]^{+}$ that are not simple superpositions of the spectra of **5** and $[\mathbf{5}]^{2+}$ strongly suggests that a class III description is appropriate for these complexes. The resolved profile has been used here to calculate the values of V_{AB} given in Table 5, which are comparable with other data reported earlier.

In the case of $[\mathbf{5}]^{+}$ the SOMO and (HOMO − 1) are orthogonal, and the IVCT band originates from one of the lower lying, predominantly metal-centered filled orbitals, to the SOMO. For the model system $[\{Ru(PH_3)_2Cp\}_2(\mu\text{-}C_4\}\}]^{+}$ we have previously calculated the energy gap between the nest of lower lying metal-centered orbitals and the SOMO to be ca. 1.4 eV, which corresponds well to the energies of the NIR bands.[8b] A referee has noted that the difference in energy between the two lower energy resolved band maxima approximates the vibrational evergy of the ν(CC) bands, and

(21) Robin, M. B.; Day, P. *Adv. Inorg. Chem. Radiochem.* **1967**, *10*, 247.
(22) Creutz, C. *Prog. Inorg. Chem.* **1989**, *30*, 1.
(23) Demadis, K. D.; Hartshorn, C. M.; Meyer, T. J. *Chem. Rev.* **2001**, *101*, 2655.
(24) (a) Nelsen, S. F. *Chem. Eur. J.* **2000**, *6*, 581. (b) Nelsen, S. F.; Tran, H. Q. *J. Phys. Chem. A* **1999**, *103*, 8139. (c) Nelsen, S. F.; Ismagilov, R. F.; Gentilr, K. E.; Powell, D. R. *J. Am. Chem. Soc.* **1999**, *121*, 7108. (d) Nelsen, S. F.; Tran, H. Q.; Nagy, M. N. *J. Am. Chem. Soc.* **1998**, *120*, 298. (e) Nelsen, S. F.; Ismagilov, R. F.; Powell, D. R. *J. Am. Chem. Soc.* **1997**, *119*, 10213.
(25) Lambert, C.; Nöll, G. *J. Am. Chem. Soc.* **1999**, *121*, 8434.
(26) Brunschwig, B. S.; Creutz, C.; Sutin, N. *Chem. Soc. Rev.* **2002**, *31*, 168.
(27) (a) Coropceanu, V.; Malagoli, M.; Andre, J. M.; Brédas, J. L. *J. Am. Chem. Soc.* **2002**, *124*, 10519. (b) Coropceanu, V.; Malagoli, M.; Andre, J. M.; Bredas, J. L. *J. Chem. Phys.* **2001**, *115*, 10409. (c) Risko, C.; Barlow, S.; Coropceanu, V.; Halik, M.; Bredas, J.-L.; Marder, S. R. *Chem. Commun.* **2003**, 194.

while vibrational structure has been observed in only a few class III systems, it is possible that the band profiles in the present systems result from vibrational fine structure rather than distinct electronic transitions.[24d,27c,28,29]

One of the goals of this work was to investigate the effects of supporting ligand(s) in a family of diyndiyl complexes **5** upon the extent to which metal and carbon orbitals are mixed. The magnitude of the comproportionation constant, K_C, is often taken as an indication of the strength of the coupling between the redox centers, and for class III complexes in which the effects of solvation on the shape and energy of the NVT band are minimal, comparison of the magnitudes of V_{AB} is also possible. In the present series, K_C and V_{AB} are similar for both the Cp*/PP derivatives [**5a/b**]$^+$ and the Cp/PR_3 complexes [**5c/d**]$^+$ (Table 3). Thus it appears that despite the increase in electron density resulting from the introduction of the Cp* and PP ligands, there has been no significant increase in the interaction between the metal centers through the C_4 bridge. However, while there is little variation in the coupling parameters within the family of complexes **5**, it should be noted that these Ru-based complexes display the largest coupling parameters observed to date in the diyndiyl series. In addition, the more highly oxidized species [**5a/b**]$^{3+/4+}$ undergo reversible redox processes, indicating that they are more stable than the analogous [**5c/d**]$^{3+/4+}$ cations studied previously.[8b]

The single-crystal X-ray structure determinations of the neutral and mono- and dicationic species **5b**, [**5b**]-[PF_6], and [**5b**][PF_6]$_2$ are of considerable interest in connection with assignments of their electronic structures. As summarized in Table 1, these data confirm the expected shortening of the Ru−C(1) and C(2)−C(3) bonds and lengthening of the C(1)−C(2) separation, consistent with the respective changes in bond order as electrons are successively removed from the HOMO, which has M−C antibonding character.[8b] This interpretation is also consistent with the infrared ν(CC) data and suggests that the 2e oxidation results in formation of the dimetalla-cumulene (**C**), as found previously in the series [{ML_n}$_2$(μ-C_4)]$^{n+}$ [n = 0−2; ML_n = MnI-(dmpe)$_2$,[3a] Re(NO)(PPh_3)Cp* [4]]. In general, the dimensions and geometry of the Ru−C_4−Ru moiety in [**5b**]$^+$ are intermediate between those of the neutral and dicationic species and point to smooth changes in these parameters as oxidation proceeds.

For the iron-based analogues of **5**, an increase in the electron density at the metal centers leads to an increased iron−iron interaction, which has been attributed to a greater overlap of metal- and carbon-based orbitals in the frontier orbitals.[7b] For the Ru systems which we have studied, electrochemical evidence suggests a more complex trend. While the first and second oxidation potentials of **5a** and **5b** are expectedly lower than those of **5c** and **5d**, more revealing is an examination of the values of $\Delta E°$ between adjacent redox steps. While $\Delta E°(1^+/2^+)$ across the series **5a**−**d** is fairly constant (0.59−0.65 V), the $\Delta E°(2+/3+)$ values are larger (0.82 and 0.89 V, respectively). These differences are significantly larger than the corresponding values measured for the analogous Cp derivatives **5c** and **5d** [$\Delta E°(2^+/3^+)$ = 0.64, 0.62 V][8b] and indicate the greater thermodynamic stabilities of the dications derived from **5a** and **5b** relative to the corresponding trications.

Our earlier computational work suggested that the frontier orbital of this species should be essentially delocalized over the six-atom Ru_2C_4 fragment.[8b] Analysis of the Hirshfield atomic charges across a series of [{Cp′L_2Ru}$_2$$C_4$]$^{n+}$ complexes suggested that there are more or less equivalent distributions of the fractional electronic charges among the atoms of the Ru−C_4−Ru bridge for n = 0, 1, 2. However, the more electron-rich (i.e., Cp*) tricationic systems (n = 3) have a greater portion of the fractional electron charge on the carbon chain than the Cp analogues.

In conclusion, we have shown that for half-sandwich ruthenium diyndiyl complexes, the use of strongly electron-donating ligands gives rise to complexes for which their higher oxidized systems are more readily available for voltammetric study than found earlier. However, the decreased chemical stability of these very highly oxidized complexes renders these species difficult to obtain on a preparative or semipreparative scale. These experiments further serve to highlight the influence of subtle variations in electronic structure, which can be engineered through control of the metal−ligand environment, have on the electronic structures of diyndiyl, and by analogy, poly-yndiyl, complexes.

Experimental Section

General Methods. All reactions were carried out under dry, high-purity nitrogen using standard Schlenk techniques. Solvents were dried, distilled, and degassed before use. Elemental analyses were from either the Canadian Microanalytical Service, Delta, B.C, Canada, or the Chemical and Micro-Analytical Services, Belmont, Victoria, Australia.

Instrumentation. Infrared: Perkin-Elmer FT-IR 1920x. Solution spectra were obtained using a 0.5 mm path length solution cell fitted with NaCl windows. Nujol mull spectra were collected from samples mounted between NaCl disks. NMR: Samples were dissolved in $CDCl_3$ (Aldrich) unless otherwise stated using 5 mm sample tubes. Spectra were recorded using either Varian Gemini 2000 (^{1}H at 300.13 MHz, ^{13}C at 75.47 MHz, ^{31}P at 121.105 MHz) or Varian Gemini 200 (^{1}H at 199.98 MHz, ^{13}C at 50.29 MHz) spectrometers. Electrospray (ES) mass spectra were measured with a Finnigan LCQ instrument, solutions in MeOH being directly infused. Cyclic voltammograms were recorded for 1.0 mM solutions in CH_2Cl_2, with 0.1 M [NBu_4][BF_4] as supporting electrolyte, using a Maclab 400 instrument. A three-electrode system was used, consisting of a platinum-dot working electrode and Pt counter and pseudo-reference electrodes. Potentials are given in V vs SCE, the ferrocene−ferricinium couple being used as internal calibrant for the measured potentials (E_0 = 0.46 V vs SCE).[30]

Reagents. The compounds HC≡$CSiMe_3$,[31] RuCl(PPh_3)$_2$-Cp*,[32] and [$FeCp_2$][PF_6][30] were prepared by standard literature methods. New syntheses of the complexes RuCl(PP)Cp* are given below. All other reagents were used as purchased from Aldrich.

Preparation of RuCl(PP)Cp*. A solution of RuCl(PPh_3)$_2$-Cp* and 1.5 equiv of the appropriate diphosphine was heated in refluxing toluene for 2 h. The hot solution was then loaded

(28) Lindeman, V.; Rosokha, S. V.; Sun, D.; Kochi, J. K. *J. Am. Chem. Soc.* **2002**, *124*, 843.
(29) Launay, J.-P. *Chem. Soc. Rev.* **2001**, *30*, 387.
(30) Connelly, N. G.; Geiger, W. E. *Chem. Rev.* **1996**, *96*, 877.
(31) Holmes, A. B.; Sporikou, C. N. *Organic Syntheses*; Wiley: New York, 1993; Collect. Vol. 8, p 606.
(32) Morandini, F.; Dondana, A.; Munari, I.; Pilloni, G.; Consiglio, G.; Sironi, A.; Moret, M. *Inorg. Chim. Acta* **1998**, *282*, 163.

directly onto a 10 × 3 cm silica column. Elution with toluene removed any free phosphine ligands. The bright orange band was eluted with 1:9 acetone/hexane, and the solvent removed to give an orange crystalline solid, which was recrystallized from CH_2Cl_2/hexane mixtures.

Compound 1a. RuCl(PPh$_3$)$_2$Cp* (100 mg, 0.12 mmol) and dppm (69 mg, 0.18 mmol) in toluene (20 mL) gave RuCl(dppm)Cp* (**1a**) (68 mg, 83%), identified from its ^{1}H NMR spectrum: δ 1.92 [t, ^4J(HP) 2.7 Hz, Cp*], 4.49, 5.16 (2 × m, 2 × 1H, CH_2), 7.53−7.78 (m, 20H, Ph) [lit. values were measured in a different solvent (d_8-thf):[16] δ 1.66 (s), 4.18 (m), 4.94 (m), 7.27−7.53 (m)]. Further spectroscopic details: ^{13}C NMR: δ 10.78 (s, Cp*), 49.09 [t, ^1J(CP) 19 Hz, CH_2], 88.61 (s, Cp*), 128.00−134.80 (m, Ph). ^{31}P NMR: δ 12.48 (s). ES mass spectrum (*m*/*z*): 621, [M − Cl]$^+$.

Compound 1b. RuCl(PPh$_3$)$_2$Cp* (100 mg, 0.12 mmol) and dppe (72 mg, 0.18 mmol) in toluene (20 mL) gave RuCl(dppe)Cp* (**1b**) (76 mg, 95%). The complex was identified from its ^{1}H NMR spectrum: δ 1.43 (s, 15H, Cp*), 2.13, 2.65 (2 × m, 2 × 2H, CH_2P), 7.18−7.68 (m, 20H, Ph) [lit. values were measured in a different solvent (d_8-thf):[16] δ 1.41 (s), 2.14 (m), 2.66 (m), 7.20−7.69 (m)]. Further spectroscopic details: ^{13}C NMR: δ 9.59 (s, C_5Me_5), 28.44 [t, J(CP) 32, CH_2], 89.00 (s, C_5Me_5), 127.38−139.03 (m, Ph). ^{31}P NMR: δ 76.25 (s). ES mass spectrum (*m*/*z*): 635, [M − Cl]$^+$.

Preparation of [Ru(=C=CH$_2$)(PP)Cp*][PF$_6$]. To a suspension of RuCl(PP)Cp* and NH_4PF_6 (2 mol equiv) in methanol was added HC≡CSiMe$_3$ (5 mol equiv), and the solution was heated at reflux point for 1 h. The resulting suspension was left to cool to room temperature before being filtered on a sintered glass frit and washed with diethyl ether (2 × 10 mL) to give a yellow crystalline solid, which was dried under vacuum.

Compound 2a. RuCl(dppm)Cp* (1375 mg, 2.12 mmol), NH_4PF_6 (694 mg, 4.25 mmol), and HC≡CSiMe$_3$ (1030 mg, 10.5 mmol) in methanol (25 mL) gave bright yellow [Ru(=C=CH$_2$)(dppm)Cp*][PF$_6$] (**2a**) (1570 mg, 96%). Anal. Calcd ($C_{37}H_{39}F_6P_3Ru$): C, 56.13; H, 4.96. Found: C, 56.49; H, 4.96. IR (Nujol, cm^{-1}): ν(C=C) 1627, ν(PF) 834. ^{1}H NMR: δ 1.77 [t, ^4J(HP) 1.8 Hz, 15H, Cp*], 3.03 [t, ^4J(HP) 3.2, 2H, CH_2], 4.63, 5.18 (2 × m, 2 × 1H, CH_2), 7.13−7.46 (m, 20H, Ph), ^{13}C NMR: δ 10.19 (s, Cp*), 48.24 [t, J(CP) 27.5, CH_2], 95.23 (s, Cp*), 102.26 (s, C_β), 127.48−135.63 (m, Ph), 344.54 [t, ^2J(CP) 14.6, C_α]. ^{31}P NMR: δ 6.56 (s), −143.6 (septet, PF_6). ES mass spectrum (*m*/*z*): 647, [Ru(CCH_2)(dppm)Cp*]$^+$; 621, [Ru(dppm)Cp*]$^+$.

Compound 2b. RuCl(dppe)Cp* (2450 mg, 3.70 mmol), NH_4PF_6 (1210 mg, 7.42 mmol), and HC≡CSiMe$_3$ (1813 mg, 18.50 mmol) in methanol (25 mL) gave bright yellow [Ru(=C=CH$_2$)(dppe)Cp*][PF$_6$] (**2b**) (2333 mg, 95%). Anal. Calcd ($C_{38}H_{41}F_6P_3Ru$): C, 56.64; H, 5.12. Found: C, 56.74; H, 5.27. IR (Nujol, cm^{-1}): ν(CC) 1621, ν(PF) 835. ^{1}H NMR: δ 1.59 [t, ^4J(HP) 1.2, 15H, Cp*], 2.58, 2.94 (2 × m, 2 × 2H, PCH_2), 2.99 [t, ^4J(HP) 1.8 Hz, 2H, CH_2], 7.09−7.57 (m, 20H, Ph). ^{13}C NMR: δ 9.76 (s, Cp*), 29.00 (m, PCH_2), 93.11 (s, Cp*), 102.65 (s, C_β), 128.61−133.75 (m, Ph), 344.21 [t, ^2J(CP) 16.4, C_α]. ^{31}P NMR: δ_p 77.28 (s), −143.6 (septet, PF_6). ES mass spectrum (*m*/*z*): 661, [Ru(CCH_2)(dppe)Cp*]$^+$; 635, [Ru(dppe)Cp*]$^+$.

Preparation of Ru(C≡CH)(PP)Cp*. To a solution of [Ru(=C=CH$_2$)(PP)Cp*][PF$_6$] in thf was added KOBu^t (1 mol equiv), and the solution was stirred at room temperature for 30 min. The solvent was removed under vacuum, and the solid was extracted in a minimum of CH_2Cl_2 and loaded onto a short (5 cm) column of basic alumina. Elution with 3:7 acetone/hexane gave a bright yellow solution, which was concentrated to give a bright yellow crystalline solid.

Compound 3a. 2a (550 mg, 0.694 mmol) and KOBu^t (78 mg, 0.694 mmol) in thf (20 mL) gave bright yellow Ru(C≡CH)(dppm)Cp* (**3a**) (420 mg, 94%). Anal. Calcd ($C_{37}H_{38}P_2Ru$): C, 68.82; H, 5.93. Found: C, 69.03; H, 5.70. IR (Nujol, cm^{-1}): ν(≡CH) 3279, ν(C≡C) 1932. ^{1}H NMR: δ 1.52 [t, ^4J(HP) 2.7, 1H, C≡CH], 1.88 [t, J(HP) 1.8 Hz, 15H, Cp*], 4.35, 4.70 (2 × td, 2 × 1H, CH_2), 7.26−7.65 (m, 20H, Ph). ^{13}C NMR: δ 10.82 (s, Cp*), 50.41 [t, J(CP) 20.1, CH_2], 91.27 [t, ^3J(CP) 3.7 Hz, Cp*], 93.01 (s, C_β), 120.26 [t, ^2J(CP) 22.8 Hz, C_α], 127.27−132.83 (m, Ph). ^{31}P NMR: δ 17.99 (s). ES mass spectrum (*m*/*z*): 647, [Ru(C_2H)(dppm)Cp* + H]$^+$, 621, [Ru(dppm)Cp*]$^+$.

Compound 3b. 2b (628 mg, 0.78 mmol) and KOBu^t (90 mg, 0.78 mmol) in thf (30 mL) gave bright yellow Ru(C≡CH)(dppe)Cp* (**3b**) (490 mg, 95%). Anal. Calcd ($C_{38}H_{40}P_2Ru$): C, 69.18; H, 6.11. Found: C, 68.79; H, 6.63. IR (Nujol, cm^{-1}): ν(≡CH) 3269, ν(C≡C) 1925. ^{1}H NMR: δ 1.54 [t, ^4J(HP) 1.6 Hz, 15H, Cp*], 1.57 [t, ^4J(HP) 2.6 Hz, 1H, ≡CH], 2.08, 2.76 (2 x m, 2 × 2H, PCH_2), 7.09−7.83 (m, 20H, Ph). ^{13}C NMR: δ 10.69 (s, Cp*), 29.90 (m, PCH_2), 92.29 [t, ^3J(CP) 2.3 Hz, Cp*], 92.99 [t, ^3J(CP) 2.3 Hz, C_β], 120.58 [t, ^2J(CP) 22.9 Hz, C_α], 127.68−137.97 (m, Ph). ^{31}P NMR: δ 82.15 (s). ES mass spectrum (*m*/*z*): 661, [Ru(C_2H)(dppe)Cp* + H]$^+$; 635, [Ru(dppe)Cp*]$^+$.

Preparation of [{Cp*(PP)Ru}$_2$(=C=CHCH=C=)][PF$_6$]$_2$. A solution of Ru(C≡CH)(PP)Cp* in CH_2Cl_2 was cooled to −78 °C. [$FeCp_2$][PF_6] (0.9 mol equiv) was added, and the mixture was stirred for 3 h at −78 °C. The product was crystallized directly from the reaction by slow addition of diethyl ether and collected by vacuum filtration, washed with further portions of diethyl ether until all excess ferrocene was removed, and dried under vacuum.

Compound 4a. 3a (940 mg, 1.44 mmol) in CH_2Cl_2 (20 mL) and [$FeCp_2$][PF_6] (450 mg, 1.38 mmol) followed by addition of diethyl ether (50 mL) gave crystalline brick red [{Cp*(dppm)Ru}$_2$(=C=CHCH=C=)][PF_6]$_2$ (**4a**) (1032 mg, 91%). The complex was recrystallized from CH_2Cl_2/hexane mixtures. Anal. Calcd ($C_{74}H_{76}F_{12}P_6Ru_2$): C, 56.21; H, 4.84. Found: C, 56.02; H, 4.71. IR (Nujol, cm^{-1}): ν(CC) 1634, ν(PF) 840. ^{1}H NMR: δ 1.78 (s, 30H, Cp*), 3.72 (s, 2H, =CH), 4.08, 5.00 (2 × m, 2 × 2H, CH_2), 6.99−7.43 (m, Ph). ^{13}C NMR: δ 10.51 (s, Cp*), 47.04 [t, ^1J(CP) 29.3 Hz, CH_2], 95.63 (s, Cp*), 102.87 (s, C_β), 128.63−134.52 (m, Ph), 348.59 [t, ^2J(CP) 15.1 Hz, C_α]. ^{31}P NMR: δ 4.76 (s), −143.6 (septet, PF_6). ES mass spectrum (*m*/*z*): 1436, [{Cp*(dppm)Ru}$_2$$C_4H_2$]$^+$; 621, [Ru(dppm)Cp*]$^+$.

Compound 4b. From **3b** (660 mg, 1.17 mmol) in CH_2Cl_2 (30 mL) and [$FeCp_2$][PF_6] (348 mg, 1.05 mmol, 0.9 mol eq), addition of diethyl ether (40 mL) crystallized brick red [{Cp*(dppe)Ru}$_2$(=C=CHCH=C=)][PF_6]$_2$ (**4b**) (685 mg, 85%). The complex was recrystallized from acetone/hexane mixtures. Anal. Calcd ($C_{76}H_{80}F_{12}P_6Ru_2$): C, 56.72; H, 5.01. Found: C, 56.77; H, 5.11. IR (Nujol, cm^{-1}): ν(CC) 1600, ν(PF) 841. ^{1}H NMR: δ 1.66 (s, 30H, Cp*), 2.57−2.78 (m, 8H, CH_2), 3.13 (s, 2H, =CH), 7.00−7.56 (m, 40H, Ph). ^{13}C NMR: δ 10.13 (s, Cp*), 28.73 (m, CH_2), 93.95 (s, Cp*), 103.22 (s, C_β), 128.79−134.41 (m, Ph), 348.08 [t, ^2J(CP) 17.8 Hz, C_α]. ^{31}P NMR: δ 75.92 (s), −143.70 (septet, PF_6). ES mass spectrum (*m*/*z*): 1465, [{Cp*(dppe)Ru}$_2$$C_4H_2$]$^+$; 635, [Ru(dppe)Cp*]$^+$.

Preparation of {Cp*(dppm)Ru}$_2$(μ-C≡CC≡C) (5a). To a solution of **4a** (640 mg, 0.4 mmol) in CH_2Cl_2 (20 mL) was added dbu (0.6 mL, 4 mmol). The solution was stirred for 15 min, after which the solvent was removed under vacuum. The oily residue was extracted with hot hexane until no more bright orange complex could be removed. The extracts were filtered and the solvent removed to give an orange crystalline solid. Trituration with cold methanol (5 mL) followed by collecting the solid on a glass sinter and washing with cold methanol (5 mL) gave {Cp*(dppm)Ru}$_2$(μ-C≡CC≡C) (**5a**) (467 mg, 90%). The analytical sample was obtained from CH_2Cl_2/hexane. Anal. Calcd ($C_{74}H_{74}P_4Ru_2$·CH_2Cl_2): C, 65.54; H, 5.57. Found: C, 65.51; H, 5.70. IR (Nujol, cm^{-1}): ν(C≡C) 1966. ^{1}H NMR (C_6D_6): δ 1.89 (s, 30H, Cp*), 4.23 (m, 4H, CH_2), 7.01−7.64 (m, 40H, Ph). ^{13}C NMR (C_6D_6): δ 11.37 (s, Cp*), 51.20 [t, ^1J(CP) 22 Hz, CH_2], 91.33 (s, Cp*), 93.25 [t, ^2J(CP) 27 Hz, C_α], 100.38 (s, C_β), 127.46−139.32 (m, Ph). ^{31}P NMR (C_6D_6): δ 17.50 (s). ES mass spectrum (*m*/*z*): 1290, [M]$^+$; 621, [Ru(dppm)Cp*]$^+$.

Preparation of {Cp*(dppe)Ru}$_2$(μ-C≡CC≡C) (5b). To a solution of **4b** (600 mg, 0.37 mmol) in thf (30 mL) was added KOBu^t (103 mg, 0.92 mmol) and the reaction stirred at room

Table 6. Crystal Data and Refinement Details

	1a	1b	2a	2b	3a	3b
formula	$C_{35}H_{37}ClP_2Ru$	$C_{36}H_{39}ClP_2Ru$	$C_{37}H_{39}F_6P_3Ru\cdot CH_2Cl_2$	$C_{38}H_{41}F_6P_3Ru$	$C_{37}H_{38}P_2Ru$	$C_{38}H_{40}P_2Ru$
MW	656.15	670.18	876.63	805.73	645.73	679.75
cryst syst	orthorhombic	monoclinic	triclinic	orthorhombic	monoclinic	monoclinic
space group	$P2_12_12_1$	$P2_1/n$	$P\bar{1}$	$Pca2_1$	$P2_1/n$	$P2_1/n$
a, Å	9.8817(9)	11.115(1)	8.8548(6)	23.4660(1)	8.8642(3)	12.4509(8)
b, Å	15.210(1)	17.767(2)	11.6736(9)	16.131(1)	32.1486(1)	19.046(1)
c, Å	20.698(2)	16.714(2)	19.309(1)	18.969(1)	11.3776(4)	13.8966(8)
α, deg			97.216(2)			
β, deg		109.131(1)	96.030(2)		107.923(1)	104.440(2)
γ, deg			102.584(2)			
V, Å^3	3111	3118	1914	7180	3084	3191
Z	4	4	2	8	4	4
D_c, g cm^{-3}	1.401	1.422	1.521	1.490	1.390	1.415
μ, cm^{-1}	7.2	7.2	7.3	6.3	6.4	6.2
cryst size, mm	0.40 × 0.15 × 0.07	0.45 × 0.37 × 0.19	0.35 × 0.10 × 0.06	0.35 × 0.30 × 0.10	0.32 × 0.07 × 0.05	0.18 × 0.15 × 0.06
$T_{min,max}$	0.42, 0.84	0.70, 0.86	0.74, 0.86	0.57, 0.77	0.74, 0.86	0.76, 0.88
$2\theta_{max}$, deg	58	58	75	58	75	75
N_{tot}	63982	29751	39689	148895	64997	67466
N_r (R_{int})	4610 (0.090)	7677 (0.018)	19734 (0.030)	9729 (0.090)	16262 (0.073)	16848 (0.083)
N_o	4160	6857	15336	7684	10026	9102
R	0.048	0.025	0.048	0.060	0.042	0.041
R_w	0.055	0.033	0.055	0.070	0.035	0.028

	4a	4b	5a	5b	[**5b**][PF_6]	[**5b**][PF_6]$_2$
formula	$C_{74}H_{76}F_{12}P_6Ru_2\cdot 4.5CH_2Cl_2$	$C_{76}H_{80}F_{12}P_6Ru_2\cdot 4C_3H_6O$	$C_{74}H_{74}P_4Ru_2\cdot C_3H_6O$	$C_{76}H_{78}P_4Ru_2\cdot C_6H_{14}$	$C_{76}H_{78}F_6P_5Ru_2$	$C_{76}H_{78}F_{12}P_6Ru_2\cdot 2H_2O$
MW	1963.58	1841.76	1347.52	1403.67	1462.46	1643.45
cryst syst	orthorhombic	monoclinic	monoclinic	triclinic	monoclinic	triclinic
space group	$C222_1$	$P2_1/c$	$P2_1/n$	$P\bar{1}$	$P2_1/n$	$P\bar{1}$
a, Å	21.716(1)	24.010(3)	14.6636(7)	10.984(2)	8.6472(8)	13.2874(9)
b, Å	24.068(2)	12.082(2)	24.461(1)	17.860(3)	20.001(2)	15.241(1)
c, Å	16.913(1)	29.331(4)	20.042(1)	17.880(3)	19.291(2)	20.520(1)
α, deg				88.906(3)		77.496(2)
β, deg		90.795(2)	111.435(1)	85.485(3)	90.794(2)	89.899(2)
γ, deg				88.576(3)		67.948(2)
V, Å^3	8840	8508	6692	3495	3336	3746
Z	4	4	4	2	2	2
D_c, g cm^{-3}	1.475	1.438	1.377	1.334	1.456	1.457
μ, cm^{-1}	7.9	5.4	5.9	5.7	6.3	6.1
cryst size, mm	0.25 × 0.23 × 0.13	0.18 × 0.08 × 0.05	0.20 × 0.15 × 0.12	0.40 × 0.30 × 0.10	0.35 × 0.14 × 0.11	0.20 × 0.15 × 0.12
$T_{min,max}$	0.75, 0.83	0.74, 0.84	0.74, 0.86	0.74, 0.86	0.73, 0.86	0.75, 0.86
$2\theta_{max}$, deg	75	58	75	58	75	58
N_{tot}	92460	82999	139241	40040	51431	72643
N_r (R_{int})	12389 (0.051)	21381 (0.056)	35201 (0.087)	16857 (0.024)	17354 (0.053)	19889 (0.046)
N_o	8288	14399	18901	13880	11199	14537
R	0.051	0.048	0.044	0.039	0.042	0.057
R_w	0.072	0.053	0.039	0.048	0.048	0.064

temperature for 30 min. The solvent was removed under vacuum and the crude solid extracted with hexane to give a bright orange solution, which was filtered through cotton wool and concentrated to give a bright orange crystalline solid. Trituration with cold ethanol (5 mL) followed by collecting on a glass sinter and washing with cold ethanol (5 mL) gave {Cp*(dppe)Ru}$_2$(μ-C≡CC≡C) (**5b**) (438 mg, 90%) as a hemi-hexane solvate. Anal. Calcd ($C_{76}H_{78}P_4Ru_2.0.5C_6H_{14}$): C, 69.74; H, 6.29. Found: C, 69.79; H, 6.40. IR (Nujol, cm^{-1}): ν(C≡C) 1973; (CH_2Cl_2): 1963. ^{1}H NMR (C_6D_6): δ 1.68 (s, 30H, Cp*), 1.95, 2.72 (2 × m, 2 × 4H, CH_2), 7.04−8.05 (m, 40H, Ph). ^{13}C NMR (C_6D_6): δ 10.09 (s, Cp*), 29.11 (s, CH_2), 92.26 (t, Cp*), 94.63 [t, ^2J(CP) 27 Hz, C$_\alpha$], 99.47 (s, C$_\beta$), 127.32−140.46 (m, Ph). ^{31}P NMR (C_6D_6): δ 82.53 (s). ES mass spectrum (m/z): 1318, [M]$^+$; 635, [Ru(dppe)Cp*]$^+$.

Preparation of [{Cp*(dppe)Ru}$_2$(C≡CC≡C)][PF$_6$]$_n$ ([5b]$^{n+}$). n = 1. To a solution of **5b** (50 mg, 0.038 mmol) in CH_2Cl_2 (20 mL) was added [$FeCp_2$][PF_6] (11.9 mg, 0.036 mmol), causing an immediate color change to bright green, after which the solution was stirred for 30 min. The solvent was concentrated under vacuum ca. 5 mL and added dropwise to hexane (250 mL) to give [{Ru(dppe)Cp*}$_2$(μ-C$_4$)][PF_6] ([**5b**][PF_6]) (48 mg, 91%) as a light green microcrystalline solid. Anal. Calcd ($C_{76}H_{78}P_5F_6Ru_2\cdot CH_2Cl_2$): C, 59.70; H, 5.21. Found: C, 59.80; H, 5.21. IR (Nujol, cm^{-1}): ν(C≡C) 1859, ν(PF) 841; (CH_2Cl_2) 1860. ^{1}H NMR: δ 6.46−7.92 (m, br, 40H, Ph), 10.72 (br, 30H, Me), 13.54 (br, 8H, CH_2P). ES mass spectrum (m/z): 1318, [{Ru(dppe)Cp*}$_2$C$_4$]$^+$; 635, [Ru(dppe)Cp*]$^+$.

***n* = 2.** To a solution of **5b** (50 mg, 0.038 mmol) in CH_2Cl_2 (20 mL) was added [$FeCp_2$][PF_6] (25 mg, 0.076 mmol) to give an immediate color change to deep blue, after which the solution was stirred for 30 min. The solvent was concentrated under vacuum (ca. 5 mL) and added dropwise to hexane (250 mL) to give [{Cp*(dppe)Ru}$_2$(C≡CC≡C)][PF_6]$_2$ ([**5b**][PF_6]$_2$) (47 mg, 79%) as a dark blue solid. Anal. Calcd ($C_{76}H_{78}P_6F_{12}Ru_2$): C, 56.79; H, 4.89. Found: C, 57.00; H, 5.02. IR (Nujol, cm^{-1}): ν(CC) 1769, ν(PF) 841; (CH_2Cl_2) 1770m, 1711vw. ^{1}H NMR (acetone-d_6): δ 1.94 (s, 30H, C$_5$*Me*$_5$), 3.01 [s (br), 8H, CH_2], 7.17−7.79 (m, 40H, Ph). ^{13}C NMR (acetone-d_6): δ 10.38 (s, C$_5$*Me*$_5$), 27.79 (m, CH_2), 112.28 (s, *C*$_5$Me$_5$), 129.80−133.97 (m, Ph). ^{31}P NMR (acetone-d_6): δ 117.89 [s (br), dppe], −143.20 (septet, PF_6). ES mass spectrum (m/z): 1463, [{Ru(dppe)Cp*}$_2$C$_4$ + PF_6]$^+$; 1318, [{Ru(dppe)Cp*}$_2$C$_4$]$^+$; 659, [{Ru(dppe)Cp*}$_2$C$_4$]$^{2+}$.

Structure Determinations. Full spheres of diffraction data were measured at ca. 153 K using a Bruker AXS CCD area-detector instrument. N_{tot} reflections were merged to N unique (R_{int} quoted) after "empirical"/multiscan absorption

correction (proprietary software), N_o with $F > 4\sigma(F)$ being used in the full matrix least squares refinement. All data were measured using monochromatic Mo Kα radiation, $\lambda = 0.71073$ Å. Anisotropic thermal parameter forms were refined for the non-hydrogen atoms, $(x, y, z, U_{iso})_H$ being constrained at estimated values. Conventional residuals R, R_w on $|F|$ are given [weights: $(\sigma^2(F) + 0.0004F^2)^{-1}$]. Neutral atom complex scattering factors were used; computation used the XTAL 3.7 program system.[33] Pertinent results are given in Figures 1−3 (which show non-hydrogen atoms with 50% probability amplitude displacement ellipsoids and hydrogen atoms with arbitrary radii of 0.1 Å) and Tables 1 and 6.

Variata. 1a. Friedel data were retained distinct, x_{abs} refining to 0.06(5). Displacement amplitudes are unreasonably high throughout the structure, suggestive of unresolved disorder or lower symmetry (etc.).

1b. The structure is isomorphous with its molybdenum analogue[34] and was refined with the same cell and coordinate setting. $(x, y, z, U_{iso})_H$ refined.

2a. Extensive disorder is found throughout the anion and solvent moieties, each being described in terms of pairs of components, occupancies set at 0.5 after trial refinement. $(x, y, z, U_{iso})_H$ refined meaningfully for the $=CH_2$ hydrogen atoms.

2b. The $=CH_2$ hydrogen atoms are postulated from the refinement behavior and chemistry. x_{abs} refined to 0.19(5).

3a. $(x, y, z, U_{iso})_H$ refined.

3b. $(x, y, z, U_{iso})_H$ refined.

4a. Anion 2 was modeled as disordered about a crystallographic 2-axis; certain solvent molecules were similarly modeled as disordered. x_{abs} refined to −0.03(4).

4b. Anion 2 was modeled as rotationally disordered about an F−P−F axis, the two sets of components of the four equatorial fluorines having occupancies refining to 0.881(6) and complement.

5b. Solvent residues were modeled in terms of hexane, C(1−3) disordered over two sets of sites, occupancies 0.5.

5b-+. $(x, y, z, U_{iso})_H$ refined.

5b-2+. Difference map residues were modeled as a pair of water molecule oxygen atoms, O···O 2.84(1) Å.

Crystallographic data for the structure determinations have been deposited with the Cambridge Crystallographic Data Centre as CCDC 190604−190615. Copies of this information may be obtained free of charge from: The Director, CCDC, 12 Union Road, Cambridge CB2 1EZ, England (fax: +44-1223-336033, e-mail: support@ccdc.cam.ac.uk, or www: http://www.ccdc.cam.ac.uk).

Acknowledgment. This work was supported by the Australian Research Council (M.I.B.) and the EPSRC (P.J.L.). B.G.E. held an Australian Post-graduate Award. We thank Johnson Matthey plc, Reading, England, for a generous loan of $RuCl_3 \cdot nH_2O$.

Supporting Information Available: X-ray structural data for **1a**/**b**, **2a**/**b**, **3a**/**b**, **4a**/**b**, **5a**/**b**, [**5b**]$^+$, and [**5b**]$^{2+}$. This material is available free of charge via the Internet at http://pubs.acs.org.

OM030015G

(33) Hall, S. R.; du Boulay, D. J.; Olthof-Hazekamp R.; Eds. *The XTAL 3.7 System*; University of Western Australia, 2000.

(34) Abugideiri, F.; Fettinger, J. C.; Keogh, D. W.; Poli, R. *Organometallics* **1996**, *15*, 4407.